Estimation of the cavity volume in the gasification zone for underground coal gasification under different oxygen flow conditions

Su, Fa-qiang
School of Energy Science and Engineering, Henan Polytechnic University

He, Xiao-long
School of Energy Science and Engineering, Henan Polytechnic University

Dai, Meng-jia
School of Energy Science and Engineering, Henan Polytechnic University

Yang, Jun-nan
School of Energy Science and Engineering, Henan Polytechnic University

他

https://hdl.handle.net/2324/7152019

出版情報：Energy. 285, pp.129309-, 2023-12-15. Elsevier
バージョン：

Energy

Estimation of the cavity volume in the gasification zone for underground coal gasification under different oxygen flow conditions

--Manuscript Draft--

Manuscript Number:	EGY-D-23-06081R2
Article Type:	Full length article
Keywords:	underground coal gasification (UCG); Stoichiometry; Cavity growth; gasification zone; Voxelization method; The Delaunay triangulation approach
Corresponding Author:	yihe yu, Ph.D Henan Polytechnic University CHINA
First Author:	Faqiang Su, Ph.D
Order of Authors:	Faqiang Su, Ph.D
	Xiaolong He
	Mengjia Dai
	Junnan Yang
	Akihiro Hamanaka
	Wen Li
	Jiaoyuan Li
	Yihe Yu
Abstract:	In this study, the impact of oxygen flow rate on the cavity of the gasification zone was analyzed through two experiments using a coaxial hole model. The oxygen flow rate was controlled between 3 L/min and 5 L/min for experiment one and between 7.5 L/min and 15 L/min for experiment two. For the estimation of the cavity volume of the gasification zone in UCG, the stoichiometric method, the Delaunay triangulation approach, and the voxelization method were used. The actual gasification zone cavity volume change was obtained by dividing the coal consumption monitored by electronic mass balance by the apparent density of the coal. After analyzing and comparing the cavity volumes of the gasification zone obtained by the three estimation methods with the actual cavity volume of the gasification zone, the results showed that the stoichiometric method had an estimation error of less than 6.5%. The Delaunay triangulation approach could reduce the estimation error for the convex cavity volume of the gasification zone to within 10%. The voxelization method could reduce the estimation error for the cavity volume of the gasification zone to below 8% and accurately describe the shape of the cavity.

Estimation of the cavity volume in the gasification zone for underground coal gasification under different oxygen flow conditions

Fa-qiang Su[a,b], Xiao-long He[a], Meng-jia Dai[a], Jun-nan Yang[a], Akihiro Hamanaka[c], Yi-he Yu[a,b,]*, Wen-Li[a], Jiao-yuan Li[a]

[a] *School of Energy Science and Engineering, Henan Polytechnic University, 2001 Century Avenue, Jiaozuo, Henan, 454-003, China*

[b] *State Collaborative Innovation Center of Coal Work Safety and Clean-efficiency Utilization, Henan Polytechnic University, Jiaozuo, Henan, 454-003, China*

[c] *Department of Earth Resources Engineering, Kyushu University, 744 Motooka, Nishi-ku, Fukuoka 819-0395, Japan*

* *Correspondence: yyhcmsj@hpu.edu.cn*

Abstract:

In this study, the impact of oxygen flow rate on the cavity of the gasification zone was analyzed through two experiments using a coaxial hole model. The oxygen flow rate was controlled between 3 L/min and 5 L/min for experiment one and between 7.5 L/min and 15 L/min for experiment two. For the estimation of the cavity volume of the gasification zone in UCG, the stoichiometric method, the Delaunay triangulation approach, and the voxelization method were used. The actual gasification zone cavity volume change was obtained by dividing the coal consumption monitored by electronic mass balance by the apparent density of the coal. After analyzing and comparing the cavity volumes of the gasification zone obtained by the three estimation methods with the actual cavity volume of the gasification zone, the results showed that the stoichiometric method had an estimation error of less than 6.5%. The Delaunay triangulation approach could reduce the estimation error for the convex cavity volume of the gasification zone to within 10%. The voxelization method could reduce the estimation error for the cavity volume of the gasification zone to below 8% and accurately describe the shape of the cavity.

Keywords:

Underground coal gasification (UCG); Stoichiometry; Cavity growth; Gasification zone; Voxelization method; The Delaunay triangulation approach

1 Introduction

Underground coal gasification (UCG) is a technology used to recover combustible gases such as H_2, CO, and CH_4 by burning coal with gasification agents (air, O_2, water vapor, etc.) delivered through injection wells. This technique is mainly applied in deep coal seams, low coal seams and unworkable coal seams by conventional methods [1-3]. As gasification proceeds, the coal is continuously consumed, and a cavity in the gasification zone will gradually form between the injection and production wells; the volume of this cavity will continue to expand as gasification proceeds, thus causing increased damage to the coal seam, which may lead to a series of problems such as gas leakage, ground subsidence, and groundwater contamination [4-7]. Therefore, it is necessary to monitor cavity expansion in the gasification zone and to estimate the volume change in the gasification zone using an efficient and accurate method.

Scholars from various countries have conducted a series of studies on the monitoring and control of Underground Coal Gasification (UCG). For example, researchers have focused on studying the combustion state in the gasification zone during cavity growth [8-11]. Additionally, many scholars have also investigated other aspects of cavity growth: Perkins et al. modeled the cavity with a packed bed model or as a free channel model, and the form of the channel was mostly considered to be cylindrical or rectangular [12-17]. Samdani et al. predicted the chamber-scale UCG cavity growth rate with an in-house developed computational fluid dynamics (CFD) model and compared it with the data obtained from chamber experiments [18-24]. Mehdi Najaf et al. used multivariate nonlinear regression analysis to establish a new model for predicting the cavity growth rate, which can be used to estimate the cavity growth rate under any given set of parameters [25]. C. Hsu, Blinderman et al. studied the formation of cavities during in situ gasification using the forward combustion linking (FCL) method [26] and determined the shape of the cavities using microfocus X-ray computed tomography [27]. Xiaopeng Liu et al. established a numerical calculation model for the temperature field inside the cavity with varying thermal parameters using the explicit finite difference method. They estimated the diffusion range of temperature inside the combustion cavity [28]. V. Prabu et al. studied the formation of UCG cavities under different experimental conditions and analyzed the results. The findings showed that the shape and formation rate of cavities were significantly affected by the oxygen flow rate, and they also highlighted the importance of ash content in cavity growth [29, 30].

It is important to understand the development of gasification zone cavities to establish safe UCG technology. As the gasification process progresses, the appearance of thermal stresses inside the coal body leads to the generation of cracks, and the locations of these cracks can be detected by acoustic emission (AE) monitoring, making it possible to monitor cavity growth using AE technology. As the cracks expand, the oxidation surface area of the coal seam increases, and combustion and gasification occur in a chain reaction-like manner. Therefore, the combustion and gasification zones will expand and move. In previous studies, AE monitoring technology was used to estimate the evolution of cavities, along with temperature monitoring and analysis of product gas composition. However, there have been few experimental studies that combine the relative energy of AE with the location of AE sources to estimate the expansion of cavities during the entire UCG process.

To achieve the objectives of this study, the stoichiometric method [31,32], the Delaunay triangulation approach [33], and the voxelization method were used to estimate the cavity volume of the gasification zone, and the relationship between coal consumption, gas composition, and temperature distribution was assessed. The stoichiometric method was used to estimate the volume of the gasification cavity by analyzing the gas composition, while the Delaunay triangulation approach and the voxelization method were used to estimate the volume of the gasification cavity by analyzing the AE source information. The stoichiometric method was used to estimate the cavity volume of the gasification zone by calculating the oxygen reaction amount and the carbon content of coal during the UCG process. The formula derivation of this method was based on the conservation of elements in the UCG chemical reaction process. Furthermore, the Delaunay triangulation approach and the voxelization method utilize AE technology as a monitoring tool to estimate the location and magnitude of AE events in the gasification zone by analyzing the waveform of elastic waves caused by thermal stress during the coal gasification process [34]. Based on this, the combustion gasification area of coal can be estimated, and the gasification zone can be visualized. The Delaunay triangulation approach, which takes the Lawson algorithm as its core idea, estimates the gasification cavity volume by constructing a tetrahedral mesh based on the source positions. On the other hand, the voxel method estimates the volume by combining the relationship between the AE source positions and the relative energy. The actual gasification zone cavity volume change was obtained by dividing the coal consumption monitored by electronic mass balance by the apparent density of the coal. The effectiveness of the three methods was verified by comparing and analyzing the estimated volumes obtained from the three methods with the actual change in gasification cavity volume.

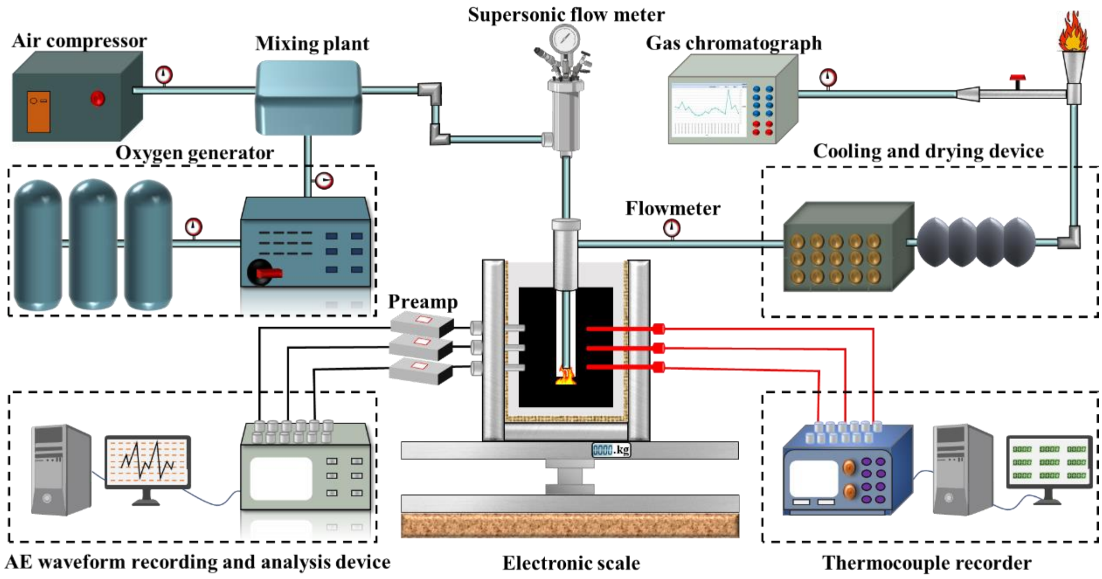

Fig. 1. Experimental system diagram.

2 Materials and methods

2.1 Experimental apparatus

The underground gasification system used in this experiment is shown in Fig. 1. The experiment was conducted using coal blocks. The coal samples were provided by Hokkaido Mining Company, Japan, and the industrial and elemental analyses of the coal samples are shown in Table 1. The whole coal body was cut and put into a sealed iron barrel (Fig. 2 a, b). The length and width of the coal body were controlled at 19~21 cm, the height was 24~26 cm, and refractory cement was poured between the coal body and the iron barrel. The entire underground gasification system was placed on an electronic mass balance, allowing real-time observation of coal mass changes during the gasification process. The gasifying agent was injected using a combination of an air compressor and an oxygen generator, with flow control achieved through the use of a supersonic flowmeter. For this experiment, the cooled product gas was passed through a synthetic gas cooling device before being cooled further and dried in a drying box to remove impurities such as tar. Temperature sensors and AE sensors were installed on both sides of the coal seam to monitor the gasification zone temperature and AE signals, respectively. The cleaned product gas was then fed into a gas chromatograph for analysis.

(a) (b) (c)

Fig. 2. Sensor arrangement, furnace body and output gas for successful ignition. (a) Coal block cutting. (b) Gasification furnace. (c) Successful ignition

Table 1 Industrial and elemental analyses of coal.

Calorific Value (MJ/kg)	Proximate Analysis (wt.%)				Ultimate Analysis (wt.%)				
	Moisture	Ash	Volatiles	Fixed Carbon	C	H	N	S	O
31.48	1.10	8.10	44.90	45.90	75.00	5.78	1.23	0.07	9.71

2.2 Experimental procedure

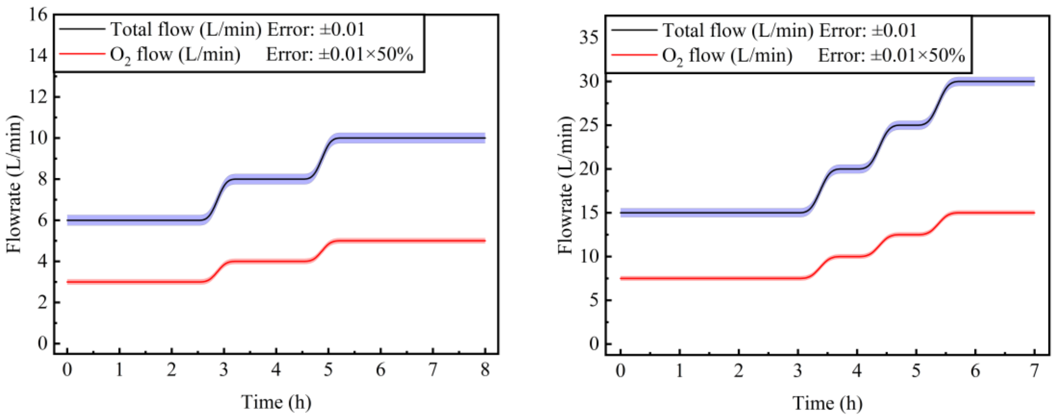

(a) (b)

Fig. 3. Feed gas flow during the gasification experiments. (a) Experiment 1. (b) Experiment 2.

For this experiment, a coaxial tube was used, which consisted of an inner and outer tube. The inner tube was used to inject a mixture of oxygen and air as the gasifying agent, while the outer tube was used to output the product gas after gasification. The distance between the tube opening and the coal bottom was 3 cm, and the diameter of the passage inside the tube was 3 cm. The experiment began by igniting the bottom of the coal with ignition materials such as sawdust, followed by the injection of a mixture of air and oxygen. The experiment used an adsorption-type oxygen making machine (product code: 20D089101) to produce oxygen. The device uses high-quality molecular sieves as adsorbents and utilizes the PSA (PRESSURE SWING ADSORPTION) variable pressure adsorption principle to directly obtain oxygen from compressed air. By mixing with the air output from the air compressor, a mixed gas with a stable oxygen concentration of 50% can be output. The ultrasonic flowmeter used in this experiment employs the principle of time difference propagation. Ultrasonic sensors are installed at two positions, upstream and downstream, to measure the speed of sound propagation from upstream to downstream and from downstream to upstream in order to calculate the fluid flow rate. In addition, the ultrasonic flowmeter includes an integrated thermometer and barometer, which can be used to correct the flow rate and pipe diameter to provide a corrected value output at standard conditions (0 ℃, 1 atm). The minimum measurable flow rate is 0.5 L/min, with a minimum measurable flow rate of 1 L/min when considering the diameter of the pipe used. Due to limitations arising from the precision of the measuring instrument and operational technique, the measurement error of the flow rate is ±0.01 L/min.

Experiment 1 was divided into three stages (1a, 1b, and 1c) based on changes in oxygen flow rate. In stage 1a (0-3 h), the oxygen flow rate was 3 L/min; in stage 1b (3-5 h), it was 4 L/min; and in stage 1c (5-8 h), it was 5 L/min. Experiment 2 was divided into four stages (2a, 2b, 2c, and 2d). In stage 2a (0-3.5 h), the oxygen flow rate was 7.5 L/min; in stage 2b (3.5-4.5 h), it was 10 L/min; in stage 2c (4.5-5.5 h), it was 12.5 L/min; and in stage 2d (5.5-7 h), it was 15 L/min, as shown in Fig. 3. The product gas was cooled and dried to remove tar and other impurities before being analyzed using a gas chromatograph. Gas composition data were recorded every half hour on average. The experiment was ended by extinguishing the fire using N_2.

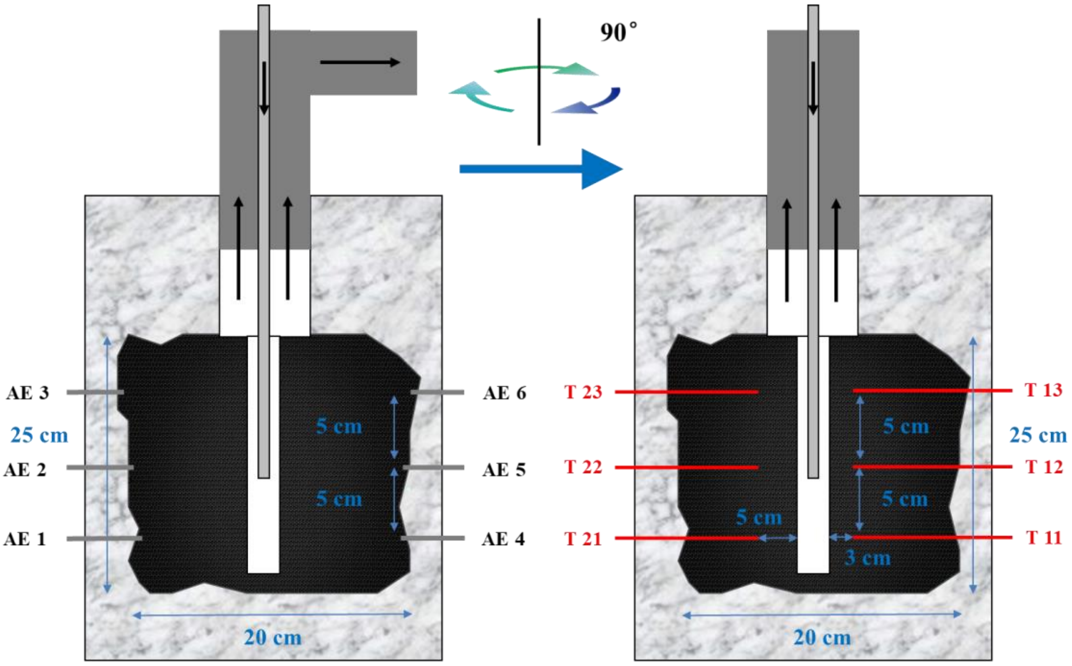

(a) (b)

Fig. 4. Layout of sensors. (a) Piezoelectric acceleration transducers. (b) Thermocouples.

Temperature changes were monitored using K-type thermocouples, which were arranged in layers according to their distance from the ignition point. The first layer, consisting of thermocouples T11 and T21, was placed near the ignition point, and subsequent layers were placed 5 cm apart from each other. The second layer consisted of thermocouples T12 and T22, and the third layer consisted of thermocouples T13 and T23, as shown in Fig. 4. Thermocouples T11-T13 on the right side of the gasification channel were placed closer to the channel at a distance of 3 cm, while thermocouples T21-T23 on the left side were placed farther away at a distance of 5 cm. AE signals were monitored using piezoelectric acceleration sensors. The physical nature of AE is the rapid release of elastic waves due to the local energy of the material. In the process of underground coal gasification, AE activity is mainly caused by thermal stress that leads to coal fracturing. The AE sensors and temperature sensors were arranged perpendicular to each other in terms of their distribution direction. All six AE sensors were inserted into the coal seam at a depth of 1 cm, as shown in Fig. 4. The thermocouples and AE sensors were arranged in the same way for both experiments. In addition, the weight of the gasifier was recorded every half hour using an electronic scale. After the experiment was completed, gypsum slurry was injected into the coal body and allowed to dry. The gasifier was then cut open along the center of the coal body, including the refractory cement.

3 Results and discussion

3.1 Relationship between coal seam temperature distribution and coal consumption

3.1.1 Monitoring of coal consumption by electronic mass balance

The entire underground gasification system was placed on an electronic scale, and the actual coal consumption during stages 1a, 1b, 1c, 2a, 2b, 2c, and 2d was monitored and is shown in Table 2 (calculated dry coal density = 0.92 g/cm^3). Overall, coal consumption in the gasification zone increased significantly with increasing oxygen flow rate, indicating that a higher oxygen flow rate leads to a faster reaction rate. Similar results, where the gasification zone cavity volume significantly increases with increasing oxygen flow rate, have been reported in the literature [30].

Table 2 Coal consumption by stage.

Experiment no.	Stage	Total time (h)	Feed flow rate (L/min)		Oxygen concentration (%)	Time interval (h)	Coal consumption (g)	Coal consumption rate (g/h)	Cavity expansion rate (cm^3/h)
			O_2	Oxygen-enriched air					
1	1a	8	3.0	6	50%	0-3	885.5	295.2	320.8
	1b		4.0	8		3-5	544.9	272.4	296.1
	1c		5.0	10		5-8	936.5	312.2	339.3
2	2a	7	7.5	15	50%	0-3.5	2270.2	648.6	705.0
	2b		10.0	20		3.5-4.5	593.7	593.7	645.3
	2c		12.5	25		4.5-5.5	630.5	630.5	685.4
	2d		15.0	30		5.5-7	1041.6	694.4	754.8

3.1.2 Temperature change

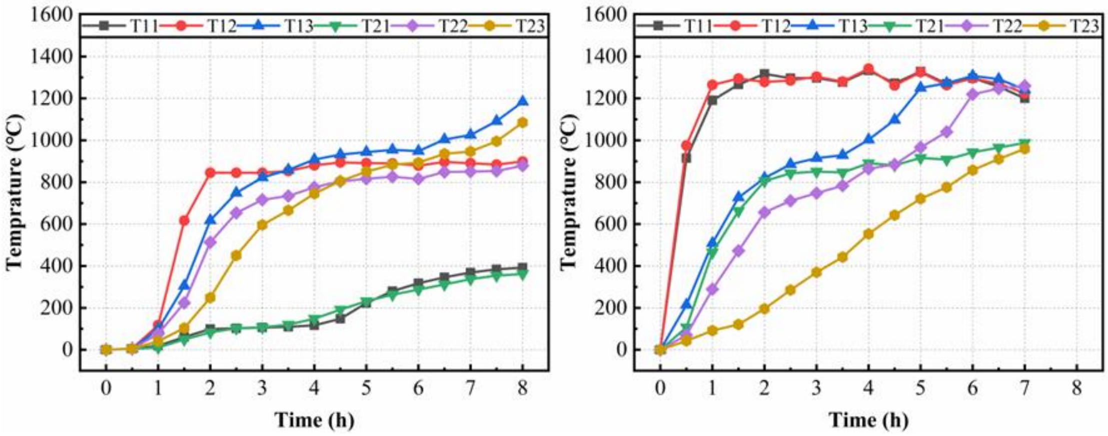

(a) (b)

Fig. 5. Temperature profiles. (a) Experiment 1. (b) Experiment 2.

Fig. 5 shows the temperature variation curves with time during the gasification process. The overall observations indicated that the coal seam temperature rose sharply in the early stage of the experiment, and the rising trend of the coal seam temperature slowed in the middle and late stages of the experiment.

Observations of temperature during experiment 1 revealed that the sharp increase in temperature did not occur at the ignition point (T11), but rather at T12 above the ignition point, where the temperature change was more dramatic than at T11. The temperature rise was particularly apparent near the gas injection port, where T12, T22, T13, and T23 showed a rapid increase, indicating that the gasification zone did not start from the area around the ignition point, but rather from the vicinity of the injection port. This may be due to the effect of the low oxygen flow rate (3 L/min), which caused the oxygen concentration at the ignition point to be lower than that near the injection port. The temperature recorded by T12 rose rapidly to approximately 800℃ at approximately 2 h, while the temperatures recorded by T11 and T21 remained below 200℃. As experiment 1 progressed to approximately 5 h and the oxygen flow rate increased (5 L/min), the temperatures of T13 and T23 above the gasification channel increased more quickly, indicating that the combustion gasification zone was expanding towards the gas outlet direction, as shown in Fig. 5(a).

In experiment 2, the temperature at the ignition point (T11) increased significantly, reaching approximately 1300℃after approximately 1 h. At the same time, with the injection of a high oxygen flow rate (7.5 L/min), the temperature of T21 at the bottom, far from the gas outlet direction also increased rapidly. This is different from the change in T21 observed in experiment 1. It can be inferred that under high flow rate conditions, the gasification zone first develops downwards from the injection port, then expands to the surrounding upper part, and finally expands outwards along the gas outlet direction, as shown in Fig. 5(b).

3.1.2 Correlation analysis between temperature and coal consumption rate

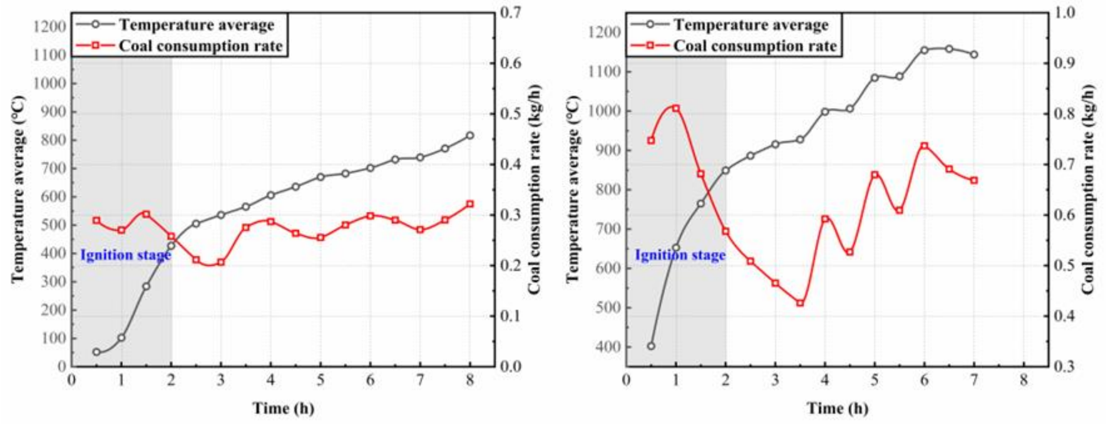

(a) (b)

Fig. 6. Relationship between temperature and coal consumption rate. (a) Experiment 1. (b) Experiment 2.

Fig. 6 shows the curves of the average temperature and coal consumption rate of the gasification zone over time for the two experiments. During the first two hours of both experiments, the gasification zone was in the ignition stage, and the gasification state was unstable. After 2 h, there was a strong correlation between the two parameters, and the coal consumption rate increased with increasing average temperature of the gasification zone. In experiment 1, the coal consumption rate peaked at 0.32 kg/h when the average temperature of the gasification zone reached its highest point of 800.3℃. In experiment 2, the coal consumption rate peaked at 0.74 kg/h when the average temperature of the gasification zone reached its highest point of 1154.8℃. We also found that the coal consumption rate changed dramatically with the changes in temperature, as seen in the period between 3.5 h and 6 h in experiment 2.

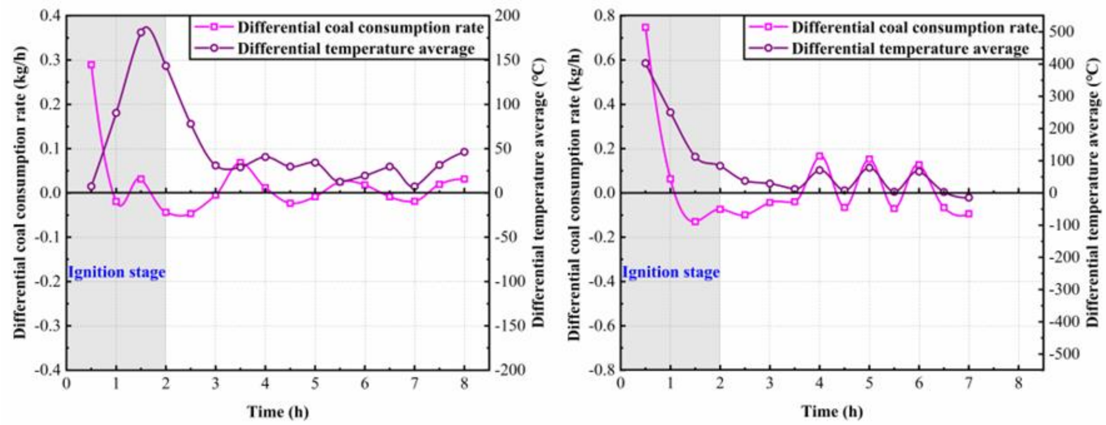

(a) (b)

Fig. 7. Differential average temperature and differential coal consumption rate curves. (a) Experiment 1. (b) Experiment 2.

By using the first-order forward difference method to analyze the coal consumption rate and average temperature data of experiments 1 and 2, we obtained Fig. 7, where the differential coal consumption rate represents the overall change in the gasification zone coal consumption rate between two adjacent time points, and the differential average temperature represents the overall change in the gasification zone temperature between two adjacent time points. From the overall trend, there is a strong correlation between the differential average temperature and the differential coal consumption rate, which is particularly evident in experiment 2. As experiment 2 progressed from stages 2a, 2b, and 2c to stages 2b, 2c, and 2d, the difference in average temperature increased by 58.4℃, 70.3℃, and 62.6℃, respectively, while the difference in coal consumption rate increased by 0.21 kg/h, 0.22 kg/h, and 0.20 kg/h. With the rapid changes in oxygen flow rate, the difference in average temperature also changed rapidly, and the difference in coal consumption rate showed the same trend as the difference in average temperature, as shown in Fig. 7(b).

3.2 Estimation of cavity growth in the gasification zone by gas composition

3.2.1 Product gas composition

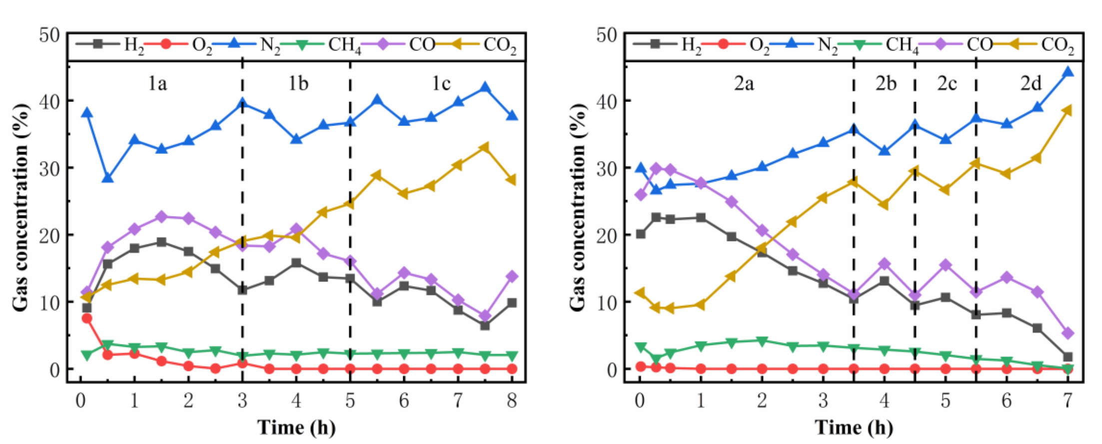

(a) (b)

Fig. 8. Composition of the gas generated during gasification. (a) Experiment 1. (b) Experiment 2.

By comparing the concentrations of CO and H_2 in the product gas at three stages of experiment 1 and four stages of experiment 2, we found that the changes in CO and H_2 concentrations were closely related to the oxygen flow rate. In stage 1a of experiment 1, the gasification zone reaction state was unstable. In stage 1b, with increases in the oxygen flow rate and in the internal temperature of the coal, there was a significant increase in CO and H_2 concentrations. After further increasing the oxygen flow rate and entering stage 1c, the concentrations of CO and H_2 showed a decreasing trend. Overall, in experiment 2, the oxygen flow rate was too high, and the concentrations of CO and H_2 in the product gas showed a decreasing trend.

3.2.2 Volume estimation based on stoichiometry

Stoichiometry was used to estimate the UCG gasification process, and the chemical reactions during the underground gasification process were represented by the elemental balance equation given in Equation (1), where H_2, CO, CO_2 and CH_4 are the main components of the dry gas, and their concentrations in the generated gas are represented by p, q, r, and s, respectively. The values of m and n were obtained through the elemental analysis of the coal sample, while α and β represent the equilibrium constants of O_2 and H_2O, respectively. γ, δ, ε, and η represent the gas yields of H_2, CO, CO_2 and CH_4, respectively.

$$CH_mO_n + \alpha O_2 + \beta H_2O \rightarrow \gamma H_2 + \sigma CO + \varepsilon CO_2 + \eta CH_4 \quad (1)$$

The gas composition of the main product gases and the stoichiometrically estimated coal consumption at different oxygen flow rates are presented in Table 3.

Table 3 Gas concentrations and coal consumption at different oxygen flow rates.

Stage	O_2 (%)	N_2 (%)	CO_2 (%)	CO (%)	CH_4 (%)	H_2 (%)	Coal consumption (g)
1a	2.3	34.04	13.43	20.80	3.27	17.96	832.1
1b	0.0	34.10	19.57	20.90	2.11	15.78	523.0
1c	0.0	36.78	26.14	14.30	2.36	12.35	889.9
2a	0.0	28.71	13.81	24.91	4.01	19.70	2133.9
2b	0.0	32.37	24.51	15.66	2.86	13.10	569.6
2c	0.0	34.09	26.71	15.48	2.06	10.64	604.1
2d	0.0	36.43	29.11	13.65	1.25	8.32	994.7

Table 4 compares the estimated cavity volume of the gasification zone obtained by stoichiometry and the actual cavity volume of the gasification zone at each stage. Due to the unstable gasification situation in the early stage of the experiment, the estimation errors of stages 1a and 2a were 6.04% and 6.0%, respectively, while the estimation errors of the other stages were all less than 5%. The best stage for estimation was stage 1b, with an estimation error of 4.01%. Overall, in experiment 1, the actual cavity volume of the gasification zone was 2572.7 cm^3, and the estimated total volume was 2440.1 cm^3, which was 5.2% smaller than the actual volume. In experiment 2, the actual cavity volume of the gasification zone was 4930.5 cm^3, and the estimated total volume was 4332 cm^3, which was 5.1% smaller than the actual volume. These results indicate that this theory can be used to estimate the gasification chamber volume accurately.

Table 4 Changes in the estimated volume by stoichiometry and the actual cavity volume of the gasification zone.

Stage	1a	1b	1c	2a	2b	2c	2d
Cavity volume by stoichiometric method (cm^3)	904.3	568.5	967.3	2319.5	619.1	656.6	1081.2
Actual cavity volume (cm^3)	962.5	592.2	1017.9	2467.6	645.3	685.4	1132.2
Error (%)	6.04	4.01	4.98	6.00	4.06	4.20	4.50

3.3 Estimation of cavity growth in the gasification zone by AE

3.3.1 AE source location calibration

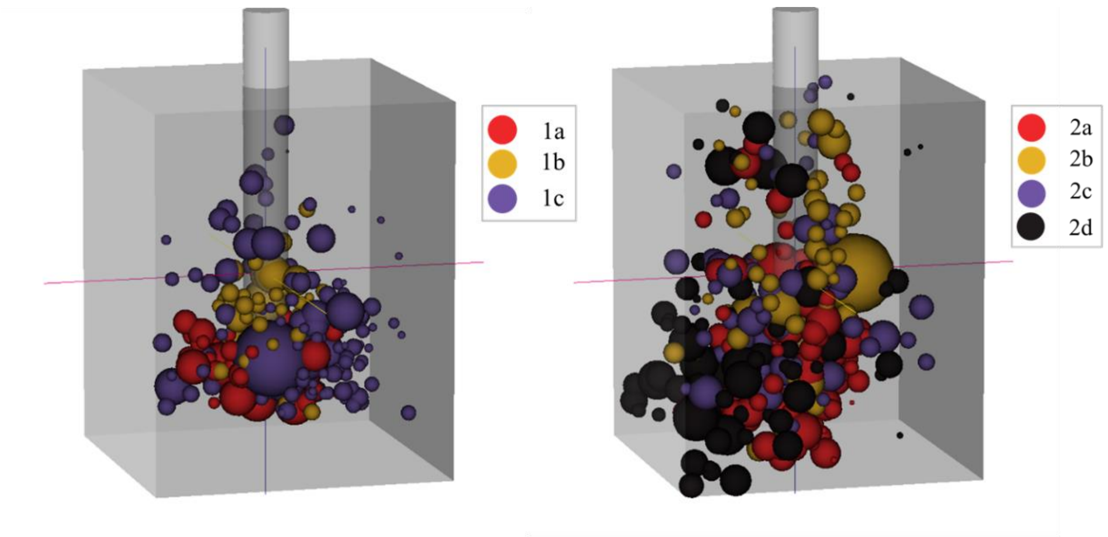

(a) (b)

Fig. 9. Results of AE source location. (a) Experiment 1. (b) Experiment 2.

The AE source location calibration results were obtained by applying the least-squares iterative algorithm [35], as shown in Fig. 9. The location of the AE source was calculated by combining the arrival time of the primary wave and the coordinates of each AE sensor. The center of the sphere represents the location of the source, and the AE events generated during different oxygen flow rate stages were divided into different phases. Experiment 1 was divided into three stages, namely, 1a, 1b, and 1c, while experiment 2 was divided into four stages, namely, 2a, 2b, 2c, and 2d. Different colors were assigned to different stages, and the size of the spheres represents the relative energy. The degree of extension of the coal seam fractures during the gasification process can be represented by the relative energy of AE, denoted as A_e, which is calculated as the square of the range of AE source energy A_0, according to Equation (2).

$$A_0 = \frac{1}{N}\sum_{j=1}^{N}(A_j \times L_j) \qquad A_e = (A_0)^2 \tag{2}$$

Here, L_j represents the distance between the calibration location of the AE source and the jth AE sensor, N is the number of AE sensors, and A_j is the maximum amplitude of the waveform obtained from the jth AE sensor.

In both experiments, the majority of the AE sources were concentrated around the coaxial hole and moved upward with time. During stages 1a and 2a, the AE sources were mainly distributed at the gas injection port and the ignition point, indicating that the fracture activity was most intense during these two stages and more cracks appeared. During stages 1b, 1c, 2b, 2c, and 2d, the fractured area mainly evolved from the gas injection port to the top gas outlet. Compared to experiment 1, experiment 2 had a larger number of large-scale AEs caused by the high oxygen flow rate, and during stage 2b, the AE sources began to spread upward in large numbers. During stages 2c and 2d, the AE sources spread to the edge of the coal seam. This phenomenon indicated that gasification started from the ignition point and gradually moved outward and upward, and high oxygen flow rates caused AE sources to spread upward more quickly.

3.3.2 Volume estimation based on the Delaunay triangulation approach

To study the cavity volume in the gasification zone, the Delaunay triangulation method was used based on the results of AE source positioning. This method is a geometric technique of combining given point source data into triangles. In this method, the circumcircle of each triangle does not contain any other point source data, so the triangles formed by each division are closest to equilateral triangles. The Delaunay triangulation method is widely used as an automatic element division method [33] in various numerical simulation software programs.

The process of 2D Delaunay triangulation began by creating a super triangle that contains all the source points and then inserting the concentrated source point data one by one. The triangle whose circumcircle contains the inserted point is called the influence triangle of that point. The common edges of the influence triangles were removed, and the inserted point was connected to all the vertices of the triangles to complete the insertion of the source data into the Delaunay triangulation data set. This process was repeated until no more points needed to be added. This step was then extended to 3D. Then, a sphere was created that contains all the source points. The maximum and minimum points of the X, Y, and Z axes in the source point data were found, and the center coordinates of each axis were calculated. When the maximum values are maxX, maxY, and maxZ and the minimum values are minX, minY, and minZ, the center coordinates centerX, centerY, and centerZ for each axis are given by Equation (3).

$$centerX = \frac{1}{2}(maxX + minX)$$

$$centerY = \frac{1}{2}(maxY + minY)$$

$$centerZ = \frac{1}{2}(maxZ + minZ) \quad (3)$$

Then, the radius was calculated using Equation (4), and by adding 0.1 to the radius, a new radius r that contained all the source point data was obtained.

$$r = \sqrt{(centerX - minX)^2 + (centerY - minY)^2 + (centerZ - minZ)^2} + 0.1 \quad (4)$$

The coordinates of the four points of the circumscribed tetrahedron, P1, P2, P3, and P4, were obtained using the center coordinates of the axis and the radius r. The coordinates of P1, P2, P3, and P4 are given by Equation (5):

$$P_1(x_{1,}\, y_{1,}\, z_{1,}) = (centerX, \quad 3r, \quad centerZ)$$

$$P_2(x_{2,}\, y_{2,}\, z_{2,}) = (centerX - 2r\sqrt{2}, \quad centerY - r, \quad centerZ)$$

$$P_3(x_{3,}\, y_3\, z_{3,}) = (centerX + r\sqrt{2}, \quad centerY - r, \quad centerZ + r\sqrt{6})$$

$$P_4(x_{4,}\, y_{4,}\, z_{4,}) = (centerX + r\sqrt{2}, \quad centerY - r, \quad centerZ - r\sqrt{6}) \quad (5)$$

Finally, the concentrated source point data were inserted one by one using a method called incremental insertion. Fig. 10 shows the tetrahedral division performed by the incremental insertion method. To determine if an inserted point was contained within the circumscribed sphere of the tetrahedron, the center coordinates O (x_0, y_0, z_0) and radius R of the circumscribed sphere were obtained using Equations (7) and (8). If the inserted source point was located inside the circumscribed sphere of the tetrahedron, the common edges of the tetrahedron were removed, and the inserted point was connected to all the vertices of the tetrahedron. This process of tetrahedral division was repeated until no more points needed to be added.

$$V = 1/6 \left\| \begin{matrix} x_2 - x_1 & y_2 - y_1 & z_2 - z_1 \\ x_3 - x_1 & y_3 - y_1 & z_3 - z_1 \\ x_4 - x_1 & y_4 - y_1 & z_4 - z_1 \end{matrix} \right\| \tag{6}$$

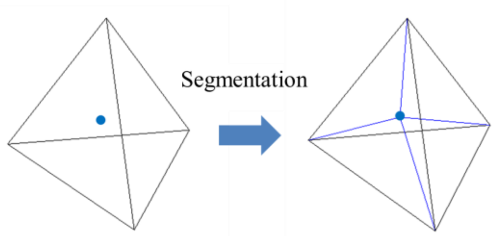

Fig. 10. The incremental insertion method was used to perform tetrahedral division.

$$x_0 = 1/120V^2 \begin{vmatrix} x_1^2 + y_1^2 + z_1^2 & y_1 & z_1 & 1 \\ x_2^2 + y_2^2 + z_2^2 & y_2 & z_2 & 1 \\ x_3^2 + y_3^2 + z_3^2 & y_3 & z_3 & 1 \\ x_4^2 + y_4^2 + z_4^2 & y_4 & z_4 & 1 \end{vmatrix}$$

$$y_0 = 1/120V^2 \begin{vmatrix} x_1^2 + y_1^2 + z_1^2 & x_1 & z_1 & 1 \\ x_2^2 + y_2^2 + z_2^2 & x_2 & z_2 & 1 \\ x_3^2 + y_3^2 + z_3^2 & x_3 & z_3 & 1 \\ x_4^2 + y_4^2 + z_4^2 & x_4 & z_4 & 1 \end{vmatrix}$$

$$z_0 = 1/120V^2 \begin{vmatrix} x_1^2 + y_1^2 + z_1^2 & x_1 & y_1 & 1 \\ x_2^2 + y_2^2 + z_2^2 & x_2 & y_2 & 1 \\ x_3^2 + y_3^2 + z_3^2 & x_3 & y_3 & 1 \\ x_4^2 + y_4^2 + z_4^2 & x_4 & y_4 & 1 \end{vmatrix} \tag{7}$$

$$R = \sqrt{(x - x_i)^2 + (y - y_i)^2 + (z - z_i)^2} \; (i = 1, 2.3, 4) \tag{8}$$

The Delaunay triangulation approach did not consider the weights of points, and it was necessary to preprocess the point cloud data. AE data with relative energy below 0.001 were regarded as small cracks and excluded, and AE data outside the coal body beyond a certain distance from the centroid of the AE source distribution was also excluded [34]. The processed AE source point cloud data were used to construct a three-dimensional tetrahedral mesh model. The basic unit of the Delaunay triangulation process was a tetrahedron, and its volume could be obtained using Equation (8). Based on the results of experiment one and experiment two, the estimated and actual changes in cavity volume of the gasification zone at various flow rates are summarized in Table 5.

Table 5 The changes in the estimated volume obtained by the Delaunay triangulation approach and the actual cavity volume of the gasification zone.

Stage	1a	1b	1c	2a	2b	2c	2d
Cavity volume determined by the Delaunay triangulation approach (cm^3)	1048.1	663.3	1252.0	2862.4	695.6	748.4	1381.2
Actual cavity volume (cm^3)	962.5	592.2	1017.9	2467.6	645.3	685.4	1132.2
Error (%)	8.90	12.00	23.00	16.00	7.80	9.20	22.00

The shapes of the cavity of the gasification zone obtained by the Delaunay triangulation approach are shown in Figs. 11 and 12. Subfigures 1a, 1b, and 1c represent the results of experiment one at 0-3 h, 0-5 h, and 0-8 h, respectively. Subfigures 2a, 2b, 2c, and 2d represent the results of experiment two at 0-3.5 h, 0-4.5 h, 0-5.5 h, and 0-7 h, respectively. As shown in Table 5, the estimation errors were all less than 25%, with a minimum of 7.8% during stage 2b. The maximum estimation error of 23% occurred during stage 1c. The reason for the estimation error may be that this method cannot describe nonconvex regions. Therefore, if the combustion zone contains nonconvex regions, this method may include them in the gasification zone, resulting in overestimation of the cavity volume and coal consumption in the gasification zone.

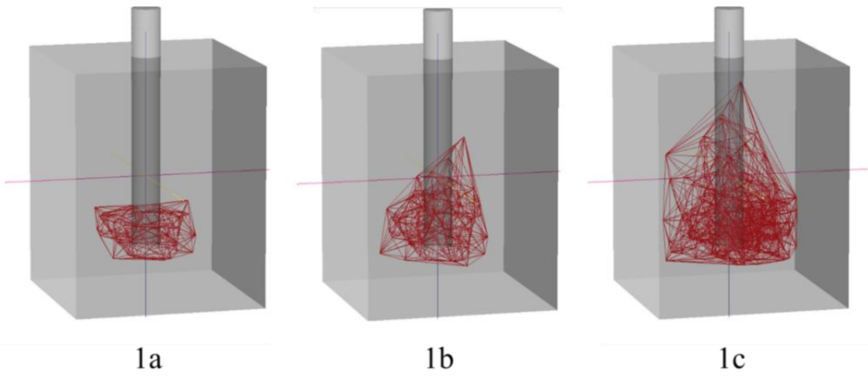

Fig. 11. Results of Delaunay triangulation to estimate the cavity of the gasification zone (Experiment 1). (1a) 0-3 h cavity effect. (1b) 0-5 h cavity effect. (1c) 0-8 h cavity effect.

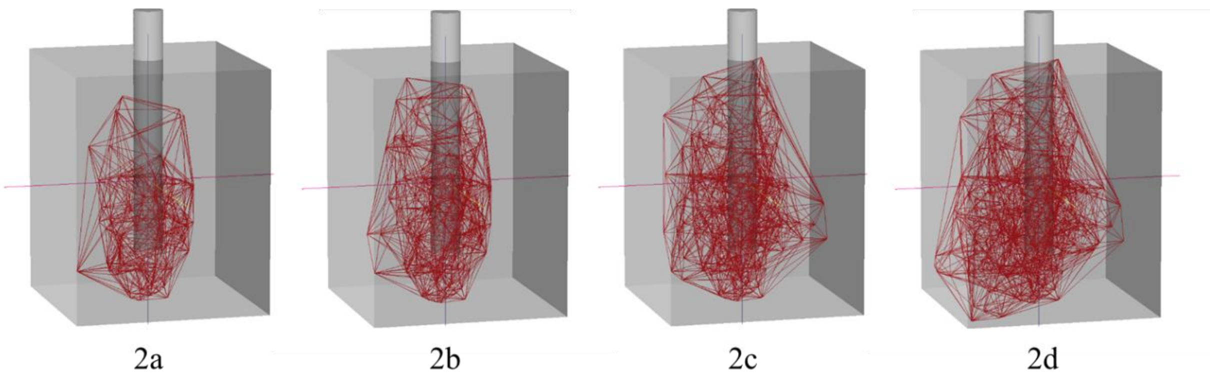

Fig. 12. Results of Delaunay triangulation to estimate the cavity of the gasification zone (Experiment 2). (2a) 0-3.5 h cavity effect. (2b) 0-4.5 h cavity effect. (2c) 0-5.5 h cavity effect. (2d) 0-7 h cavity effect.

3.3.3 Volume estimation based on the Delaunay triangulation approach

Due to the limitations of the Delaunay triangulation approach in estimating the cavity volume of the gasification zone and its inability to describe nonconvex regions, the point cloud data used in this study considered only the AE source point coordinates and did not consider other AE data. To minimize errors, a voxel-based method was proposed for volume evaluation. This method can describe nonconvex regions and considers the relative energy of AE as the weight of the point. Voxels with a size corresponding to the relative energy of AE were assigned to the source points to represent the cavity volume of the gasification zone.

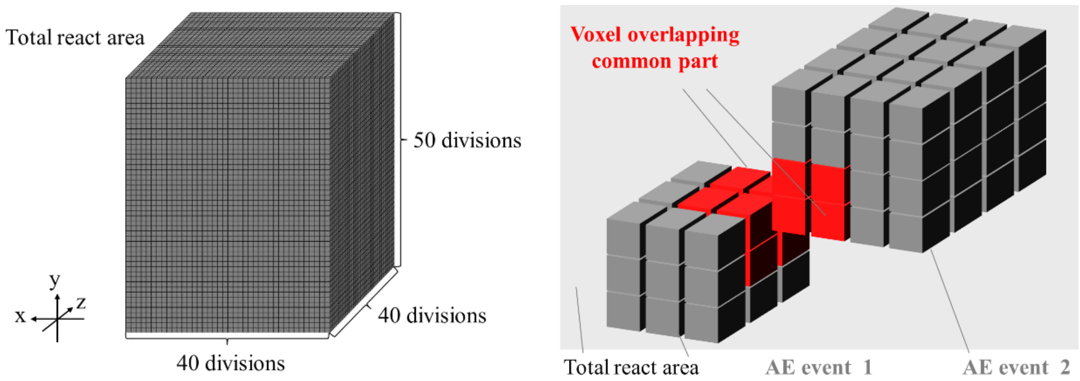

(a) (b)

Fig. 13. Voxel representation method. (a) 3D mesh segmentation of the coal body. (b) Overlap of voxels.

In the voxelization method, the coal body was divided into a three-dimensional grid with 40 divisions in the x and z directions and 50 divisions in the y direction, creating a total of 40 × 40 × 50 cubes, as shown in Fig. 13(a). Each cube is called a voxel, and each voxel was assigned a volume of 0.125 cm^3 (the original coal body was 20 × 20 × 25 cm^3, and each voxel's volume is equivalent to 1/80,000 of the original coal body). Based on the relative energy of AE within a certain range, values were input into the voxels, as shown in Fig. 13(b), which displays the data for two different AE source points with energy sizes of 3 × 3 × 3 and 4 × 4 × 4 voxels. The common portion of the two source points is the overlapping section (2 × 2 × 2 voxels), and the advantage of this method is that the overlapping section is not double-counted when assigning values to the voxels. This method can accurately estimate the cavity volume in the gasification zone, thereby accurately estimating the coal consumption. The sum of the values input into the voxels was used as the volume of the reactive coal.

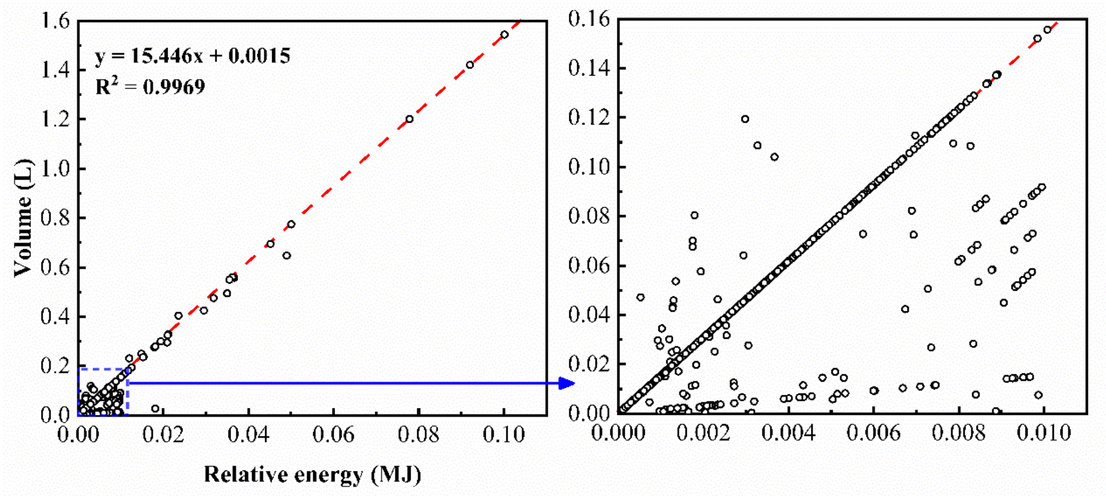

(a) (b)

Fig. 14. (a) Relative energy vs. volume. (b) Relative energy vs. volume. (Relative energy is below 0.011)

In this method, the relative energy data of the AE source points and the actual gasification zone volume data from the two experiments were analyzed and compared. It was found that the relationship between the two data sets was well described by a linear function. Thus, a linear regression was performed to derive an empirical formula that related the actual cavity volume in the gasification zone to the relative energy of the AE source points. The relative energy of the AE source points and the estimated volume were linearly correlated with a correlation coefficient of 0.996, as shown in Fig. 14.

Fig. 14 shows that the data points with relative energy values below 0.011 were more scattered than those with relative energy values above 0.011. Therefore, an error analysis was performed separately for the data points with relative energy values below 0.011. The points that deviated from the fitting curve corresponded to 7.8% of the total number of AE events, and the associated volume accounted for 9.6% of the total volume corresponding to all AE events with relative energy values below 0.011. In terms of the total number of events, the points that deviated from the fitting curve corresponded to 7.2% of the total number of AE events, and the associated volume accounted for 4.1% of the total volume corresponding to all AE events.

Using the empirical formula obtained from Fig. 14, the cavity volume changes in the gasification zone at various oxygen flow rates in the two experiments were estimated. The voxel-based method was used to estimate the cavity volume changes at each flow rate, and the results were compared with the actual cavity volume changes, as shown in Table 6. The estimation error was the smallest during stage 2d, with a maximum error of 4.0%. The maximum error of stage 2a was 10.1%, and the errors in each stage were less than 11%, indicating that the AE source point position information combined with the relative energy can indeed accurately estimate the cavity volume of the gasification zone.

Table 6 The changes in the estimated volume obtained by the voxelization method and the actual cavity volume of the gasification zone.

Stage	1a	1b	1c	2a	2b	2c	2d
Cavity volume by the voxelization method (cm^3)	1022.1	634.9	1081.0	2716.8	684.0	716.2	1177.4
Actual cavity volume (cm^3)	962.5	592.2	1017.9	2467.6	645.3	685.4	1132.2
Error (%)	6.20	7.20	6.20	10.10	6.00	4.50	4.00

The morphology of the gasification zone obtained by the voxelization method is shown in Figs. 15 and 16. Subfigures 1a, 1b, and 1c represent the voxel results for experiment 1 at 0-3 h, 0-5 h, and 0-8 h, respectively. Subfigures 2a, 2b, 2c, and 2d represent the voxel results for experiment 2 at 0-3.5 h, 0-4.5 h, 0-5.5 h, and 0-7 h, respectively.

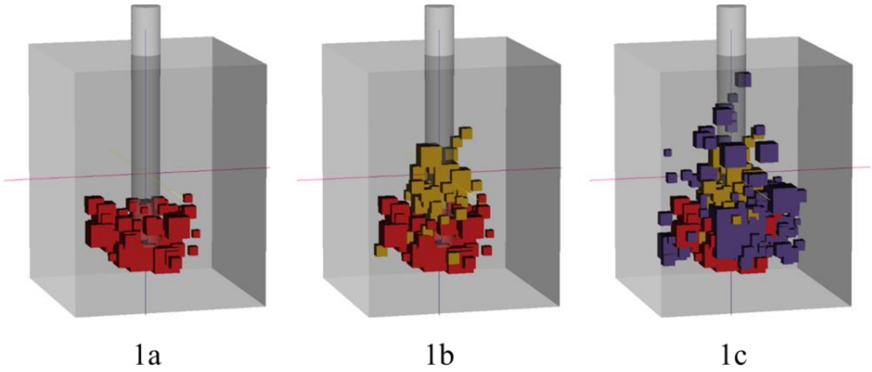

Fig. 15. Results of the voxelization method to estimate the cavity of the gasification zone (Experiment 1). (1a) 0-3 h cavity effect. (1b) 0-5 h cavity effect. (1c) 0-8 h cavity effect.

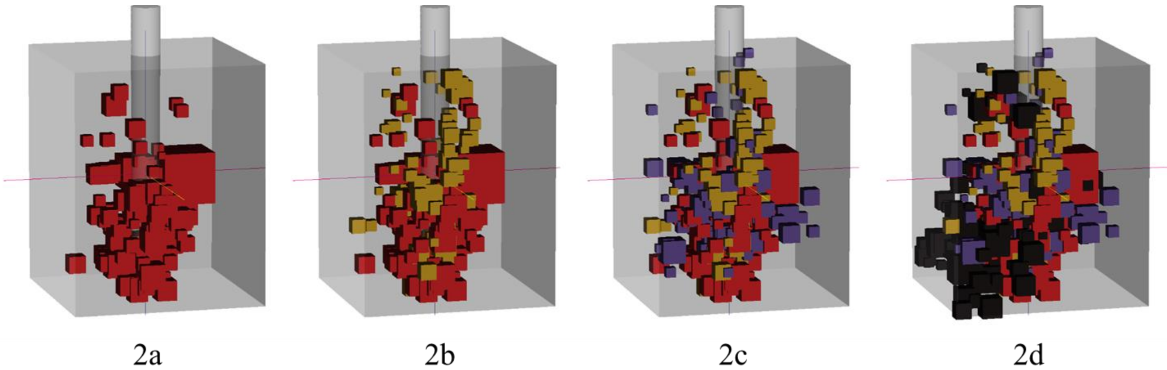

Fig. 16. Results of the voxelization method to estimate the cavity of the gasification zone (Experiment 2). (2a) 0-3.5 h cavity effect. (2b) 0-4.5 h cavity effect. (2c) 0-5.5 h cavity effect. (2d) 0-7 h cavity effect.

3.3.4 Model Errors and Limitations

In summary, the chemical stoichiometry method, Delaunay triangulation method, voxel method, and weighing method are used to calculate the expansion velocity of the gasification cavity. The limitations of the chemical stoichiometry method include the lack of consideration for tar filtered by the filtration system and volatile substances present during the gasification process. As shown in Figure 17(a), this estimation method generally underestimates the expansion velocity of the cavity, with a maximum estimation error of 6.04% in Stage 1a and a minimum estimation error of 4.01% in Stage 1b. Furthermore, the chemical stoichiometry method cannot estimate the shape of the gasification cavity.

As for limitations, the Delaunay triangulation method is not suitable for nonconvex sets. Nonconvex sets have complex topological structures in their boundary regions, making it impossible to establish a continuous and reasonable triangular mesh through nearest neighbour relationships. It may also generate triangles with extreme shapes, leading to overestimated results. As shown in Figure 17(b), this method generally overestimates the expansion velocity of the cavity, with a maximum estimation error of 23% in Stage 1c and a minimum estimation error of 7.8% in Stage 2b.

The limitation of the voxel method lies in the fact that the size of the voxels affects the accuracy and resolution of the estimation results. If the voxels are too large, they cannot accurately describe the detailed structures within the cavity, resulting in inaccurate estimation results. If the voxels are too small, the computational complexity and storage requirements will increase. As shown in Figure 17(c), this method generally overestimates the expansion velocity of the cavity, with a maximum estimation error of 10.1% in Stage 2a and a minimum estimation error of 4.0% in Stage 2d. Additionally, both the voxel method and triangulation method are greatly influenced by the accuracy of acoustic emission for rupture monitoring rather than the algorithms themselves. Improving the accuracy of acoustic emission for rupture monitoring will effectively enhance the accuracy of these two prediction models.

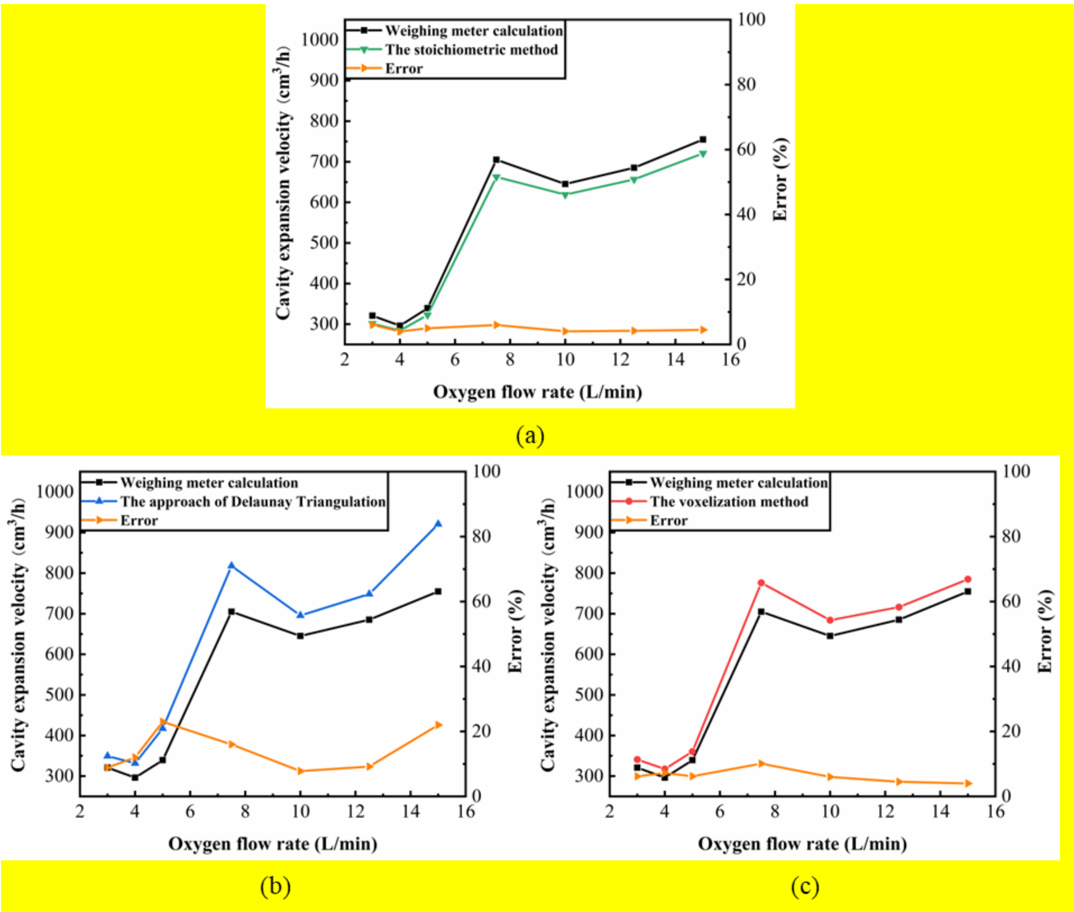

Fig. 17. The actual value of cavity expansion rate and the estimated value of the gasification zone. (a) The stoichiometric method (b) The Delaunay triangulation approach (c) The voxelization method

After the experiment, we cut the coal sample along the center and compared the profiles obtained by the Delaunay triangulation approach and the voxelization methods, as shown in Fig. 18. The typical nonconvex areas are highlighted using yellow circles. For experiment 1, the voxelization method had an estimation error of 6.4% for the cavity volume in the gasification zone at the end of the experiment, while the Delaunay triangulation approach had an error of 15.2%. Therefore, the voxelization method was 8.8% more accurate than the Delaunay triangulation approach. For experiment 2, the voxelization method had an estimation error of 7.4%, while the Delaunay triangulation approach had an error of 15.4%. Therefore, the voxelization method was 8% more accurate than the Delaunay triangulation approach. From the profiles of the areas numbered 1-3 in the figure, it can be seen that the voxelization method has advantages in estimating the cavity volume of the gasification zone and describing the shape of the cavity and can better address the problems of the Delaunay triangulation approach in overestimating the volume due to inaccurate shape description of nonconvex areas. Finally, the error calculated by overlapping the profile with the triangulation image and the voxelized image is shown in Table 7. It is found that the estimation of section area by triangulation method is closer to the original section area. The reason we speculate here is that the original section actually contains a portion of the unvaporized area, which would be accounted for by triangulation, but not by voxel. In the future, we will consider improving the grouting material and filling the cavity with more suitable materials to ensure higher accuracy.

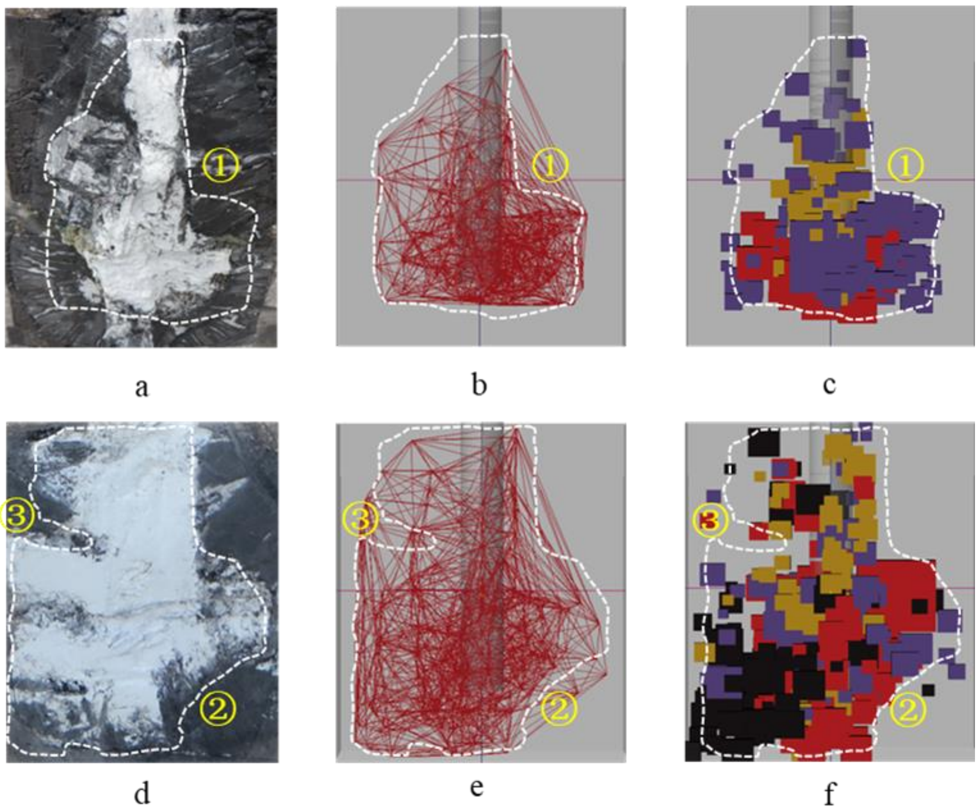

Fig. 18. (a) Actual profile (Experiment 1). (b) Profile obtained by the Delaunay triangulation approach (Experiment 1). (c) Profile obtained by the voxelization method (Experiment 1). (d) Actual profile (Experiment 2). (e) Profile obtained by the Delaunay triangulation approach. (Experiment 2). (f) Profile obtained by the voxelization method (Experiment 2).

Table 7 To compare the section area obtained through voxelization and triangulation with the section area obtained from actual cutting.

Section type	Experiment 1	Experiment 2
Section area by the Delaunay triangulation approach (cm^2)	246.00	396.90
Section area by the voxelization method (cm^2)	236.10	350.52
Actual section area (cm^2)	267.06	397.74
Error (the Delaunay triangulation approach) (%)	-7.89	-0.21
Error (the voxelization method) (%)	-11.59	-11.87

4. Conclusion

(1) The oxygen flow rate in the gasification agent is one of the main factors affecting the coal consumption rate in gasification. Overall, as the oxygen flow rate increases, the coal consumption rate significantly increases. Specifically, when the oxygen flow rate increased from 3 L/min to 15 L/min, the coal consumption rate increased from 295.2 g/h to 694.4 g/h. Moreover, there is a strong correlation between the differential average temperature and differential coal consumption rate. With drastic changes in oxygen flow rate, the differential average temperature quickly changes, and the differential coal consumption rate shows the same trend as the differential average temperature.

(2) AE monitoring combined with Delaunay triangulation is a useful means of visualizing the three-dimensional gasification zone. As the number of AE sources increases, the Delaunay triangulation approach can estimate the shape of the gasification zone in different flow rate stages in real time. The combination of AE monitoring and the Delaunay triangulation approach has good performance in estimating the cavity volume of the convex gasification zone. Specifically, when the oxygen flow rate is 3 L/min, the estimation error is 8.9%, and when the oxygen flow rate is 10 L/min, the estimation error is 7.8%. According to past underground gasification experiments, a convex gasification zone is generally formed under good experimental conditions. Therefore, this method is suitable for estimating the volume of the convex gasification zone.

(3) Compared with the Delaunay triangulation approach, the voxelization method is more effective in estimating the cavity volume of the gasification zone and describing the cavity shape. In terms of estimating the cavity volume of the gasification zone, in experiment 1, the voxelization method had an error of 6.4% after the experiment was completed, while the Delaunay triangulation approach had an error of 15.2%. The voxelization method improved the accuracy by 8.8% compared to the Delaunay triangulation approach. In experiment 2, the voxelization method had an error of 7.4% after the experiment was completed, while the Delaunay triangulation approach had an error of 15.4%. The voxelization method improved the accuracy by 8% compared to the Delaunay triangulation approach. From the comparison of the gypsum profiles in the later stage of the experiment, the voxelization method can describe the cavity shape more accurately.

(4) The stoichiometric method, the Delaunay triangulation approach, and the voxelization method each have their own advantages and disadvantages. The stoichiometric method has good overall

performance in estimating the cavity volume, with small errors, but it cannot describe the three-dimensional shape of the gasification zone. The Delaunay triangulation approach is suitable for evaluating the cavity of the convex gasification zone. The voxelization method can provide a more accurate estimation of the cavity volume and the three-dimensional shape of the gasification zone based on an empirical relationship supported by preliminary experimental data for a specific type of underground gasification experiment. The three methods can be used in combination to effectively and accurately estimate the changes in the cavity of the gasification zone.

Credit author statement

Fa-qiang Su.: Investigation, Writing-Reviewing and Editing, Funding acquisition. Xiao-long He: Investigation, Writing-Original draft preparation, Funding acquisition. Meng-jia Dai: Supervision, Validation. Jun-nan Yang: Investigation, Data curation. Akihiro Hamanaka: Conceptualization, Methodology. Yi-he Yu: Investigation, Validation, Data curation, Funding acquisition. Wen-Li: Investigation, Validation. Jiao-yuan Li: Validation, Resources.

Declaration of Competing Interest

The authors declare that they have no known competing financial interests or personal relationships that could have appeared to influence the work reported in this paper.

Data availability

Data will be made available on request.

Acknowledgments

This work was supported by Key Laboratory of Western Mine Exploitation and Hazard Prevention, Ministry of Education (SKLCRKF1902), State Key Laboratory for Geomechanics and Deep Underground Engineering, China University of Mining & Technology (SKLGDUEK2004), Key R & D and promotion projects (scientific and technological breakthrough) in Henan Province (16220043), Key Scientific Research Project of Colleges and Universities in Henan Province (22B440003), Natural Science Foundation of Henan Province of China (232300421205). The authors gratefully acknowledge their support, and expresses particular appreciation to UCG project members.

References:

[1] Olateju, B. and A. Kumar, Techno-economic assessment of hydrogen production from underground coal gasification (UCG) in Western Canada with carbon capture and sequestration (CCS) for upgrading bitumen from oil sands. Applied Energy, 2013. 111(10): p. 428-440. https://doi.org/10.1016/j.apenergy.2013.05.014

[2] Prabu, V. and S. Jayanti, Underground coal-air gasification based solid oxide fuel cell system. Applied Energy, 2012. 94: p. 406-414. https://doi.org/10.1016/j.apenergy.2012.01.040

[3] Bhutto, A.W., A.A. Bazmi and G. Zahedi, Underground coal gasification: From fundamentals to applications. Progress in Energy and Combustion Science, 2013. 39(1): p. 189-214. https://doi.org/10.1016/j.pecs.2012.09.004

[4] A C L , A H C , B C J ,et al.A back analysis of the temperature field in the combustion volume space during underground coal gasification[J]. 2011, 21(4):5.DOI:10.1016/j.mstc.2011.06.018.

[5] Mallett CW. Environmental controls for underground coal gasification. Proc IMechE Part A: J Power & Energy 2017. https://doi: 10.1177/0957650917723733.

[6] Derbin Y, Walker J, Wanatowski D, Marshall A. Soviet experience of underground coal gasification focusing on surface subsidence. J Zejiang Univ 2015;16:839–50. https://doi: 10.1631/jzus.A1500013.

[7] Mehdi, Najafi Seyed, et al. Prediction of cavity growth rate during underground coal gasification using multiple regression analysis[J]. Int J Coal Sci Technol 2015; 2(4):318–24. https://doi.org/10.1007/s40789-015-0095-9

[8] Khan, M.M.; Mmbaga, J.P.; Shirazi, A.S.; Trivedi, J.; Liu, Q.; Gupta, R. Modelling Underground Coal Gasification—A Review. Energies 2015, 8, 12603–12668. https://doi.org/10.3390/en81112331

[9] Nourozieh, H.; Kariznovi, M.; Chen, Z.; Abedi, J. Simulation Study of Underground Coal Gasification in Alberta Reservoirs: Geological Structure and Process Modeling. Energy Fuels 2010, 24, 3540–3550. https://doi.org/10.1021/ef9013828

[10] Cui, Y.; Liang, J.; Wang, Z.; Zhang, X.; Fan, C.; Liang, D.; Wang, X. Forward and reverse combustion gasification of coal with production of high-quality syngas in a simulated pilot system for in situ gasification.Appl. Energy 2014, 131, 9–19. https://doi.org/10.1016/j.apenergy.2014.06.001

[11] Daggupati, S.; Mandapati, R.N.; Mahajani, S.M.; Ganesh, A.; Mathur, D.K.; Sharma, R.K.; Aghalayam, P. Laboratory studies on combustion cavity growth in lignite coal blocks in the context of underground coal gasification. Energy 2010, 35, 2374–2386. https://doi.org/10.1016/j.energy.2010.02.015

[12] Perkins, G. and V. Sahajwalla, Steady-State Model for Estimating Gas Production from Underground Coal Gasification. Energy & Fuels, 2008. 22(6): p. 3902-3914. https://doi.org/10.1021/ef8001444

[13] Perkins, G. and V. Sahajwalla, A Numerical Study of the Effects of Operating Conditions and Coal Properties on Cavity Growth in Underground Coal Gasification. Energy & Fuels, 2006. 20(2): p. 81 - 88. https://doi.org/10.1021/ef050242q

[14] Yang, L., Study on the model experiment and numerical simulation for underground coal gasification. Fuel, 2004. 83(4/5): p. 573-584.https://doi.org/10.1016/j.fuel.2003.08.011
[15] Khadse, A.N., et al., Reactor Model for the Underground Coal Gasification (UCG) Channel. International Journal of Chemical Reactor Engineering, 2006. 4(1). https://doi.org/10.2202/1542-6580.1351
[16] Nourozieh, H., et al., Simulation Study of Underground Coal Gasification in Alberta Reservoirs: Geological Structure and Process Modeling. Energy & Fuels, 2010. 24(MAY-JUN.): p. 3540-3550. https://doi.org/10.1016/j.cherd.2012.11.008
[17] Daggupati, S., et al., Compartment Modeling for Flow Characterization of Underground Coal Gasification Cavity. Industrial & Engineering Chemistry Research, 2011. 50(1): p. 277-290. https://doi.org/10.1021/ie101307k
[18] Sarndani, G., et al., A process model for underground coal gasification – Part-III: Parametric studies and UCG process performance. Fuel, 2018. 234(DEC.15): p. 392-405. https://doi.org/10.1016/j.fuel.2018.07.011
[19] Samdani, G., et al., A process model for underground coal gasification – Part-II growth of outflow channel. Fuel, 2016. 181: p. 587-599.https://doi.org/10.1016/j.fuel.2016.05.017
[20] Samdani, G., et al., A process model for underground coal gasification – Part-I: Cavity growth. Fuel, 2016. 181(oct.1): p. 690-703.https://doi.org/10.1016/j.fuel.2016.05.020
[21] Gao, W., et al., Simulation of underground coal gasification based on a coupled thermal-hydraulic-chemical model. Combustion theory and modelling, 2022(1): p. 26. https://doi.org/10.1080/13647830.2021.1992507
[22] Xin, L., et al., Theoretical research on heat transfer law during underground coal gasification channel extension process. International Journal of Heat and Mass Transfer, 2019. 142(OCT.): p. 118409.1-118409.14.https://doi.org/10.1016/j.ijheatmasstransfer.2019.07.059
[23] Shahbazi, M., M. Najafi and M.F. Marji, On the mitigating environmental aspects of a vertical well in underground coal gasification method. Mitigation and Adaptation Strategies for Global Change, 2019. 24. https://doi.org/10.1007/s11027-018-9816-x
[24] Cheng W , Xin L , Wang G ,et al.Analytical research on dynamic temperature field of overburden in goaf fire-area under piecewise-linear third boundary condition[J].International Journal of Heat & Mass Transfer, 2015, 90(nov.):812-824.DOI:10.1016/j.ijheatmasstransfer.2015.07.012.
[25] Najafi, M., et al., Prediction of cavity growth rate during underground coal gasification using multiple regression analysis. International Journal of Coal Science & Technology, 2015. 2(004): p. 318-324.https://doi.org/10.1007/s40789-015-0095-9
[26] Blinderman, M.S., D.N. Saulov and A.Y. Klimenko, Forward and reverse combustion linking in underground coal gasification. Energy, 2008. 33(3): p. 446-454. https://doi.org/10.1016/j.energy.2007.10.004
[27] Hsu, C., et al., Investigation of cavity formation in lump coal in the context of underground coal gasification. Journal of the Southern African Institute of Mining & Metallurgy, 2014. 114(4): p. 305-309. DOI:10.1016/j.energy.2010.02.015.
[28] Liu, X., G. Guo and H. Li, Study on the Propagation Law of Temperature Field in Surrounding

Rock of Underground Coal Gasification(UCG) Combustion Cavity Based on Dynamic Thermal Parameters. Results in Physics, 2019. 12. https://doi.org/10.1016/j.rinp.2019.02.006

[29] Prabu, V. and S. Jayanti, Heat-affected zone analysis of high ash coals during ex situ experimental simulation of underground coal gasification. Fuel, 2014. 123(may 1): p. 167-174. https://doi.org/10.1016/j.fuel.2014.01.035

[30] Prabu, V. and S. Jayanti, Simulation of cavity formation in underground coal gasification using bore hole combustion experiments. Energy, 2011. 36(10): p. 5854-5864. https://doi.org/10.1016/j.energy.2011.08.037

[31] Su, F.Q., et al., Monitoring and evaluation of simulated underground coal gasification in an ex-situ experimental artificial coal seam system. Applied Energy, 2018. 223(AUG.1): p. 82-92. https://doi.org/10.1016/j.apenergy.2018.04.045

[32] Su F Q , Zhang T , Wu J B ,et al.Energy recovery evaluation and temperature field research of underground coal gasification under different oxygen concentrations[J].Fuel: A journal of fuel science, 2022. https://doi.org/10.1016/j.fuel.2022.125389

[33] Fa-qiang, et al., Evaluation of Coal Combustion Zone and Gas Energy Recovery for Underground Coal Gasification (UCG) Process. Energy & Fuels, 2016. 31(1): p. 154-169. https://doi.org/10.1021/acs.energyfuels.6b01922

[34] Su, F.Q., et al., Monitoring of coal fracturing in underground coal gasification by acoustic emission techniques. Applied Energy, 2017. 189(MAR.1): p. 142-156. https://doi.org/10.1016/j.apenergy.2016.11.082

[35] Tribikram Kundu. Acoustic source localization (Ultrasonics, vol. 54, issue 1) (2013). https://doi.org/10.1016/j.ultras.2013.06.009

Estimation of the cavity volume in the gasification zone for underground coal gasification under different oxygen flow conditions

Fa-qiang Su[a,b], Xiao-long He[a], Meng-jia Dai[a], Jun-nan Yang[a], Akihiro Hamanaka[c], Yi-he Yu[a,b,*], Wen-Li[a], Jiao-yuan Li[a]

[a] *School of Energy Science and Engineering, Henan Polytechnic University, 2001 Century Avenue, Jiaozuo, Henan, 454-003, China*

[b] *State Collaborative Innovation Center of Coal Work Safety and Clean-efficiency Utilization, Henan Polytechnic University, Jiaozuo, Henan, 454-003, China*

[c] *Department of Earth Resources Engineering, Kyushu University, 744 Motooka, Nishi-ku, Fukuoka 819-0395, Japan*

* *Correspondence: yyhcmsj@hpu.edu.cn*

Abstract:

In this study, the impact of oxygen flow rate on the cavity of the gasification zone was analyzed through two experiments using a coaxial hole model. The oxygen flow rate was controlled between 3 L/min and 5 L/min for experiment one and between 7.5 L/min and 15 L/min for experiment two. For the estimation of the cavity volume of the gasification zone in UCG, the stoichiometric method, the Delaunay triangulation approach, and the voxelization method were used. The actual gasification zone cavity volume change was obtained by dividing the coal consumption monitored by electronic mass balance by the apparent density of the coal. After analyzing and comparing the cavity volumes of the gasification zone obtained by the three estimation methods with the actual cavity volume of the gasification zone, the results showed that the stoichiometric method had an estimation error of less than 6.5%. The Delaunay triangulation approach could reduce the estimation error for the convex cavity volume of the gasification zone to within 10%. The voxelization method could reduce the estimation error for the cavity volume of the gasification zone to below 8% and accurately describe the shape of the cavity.

Keywords:

Underground coal gasification (UCG); Stoichiometry; Cavity growth; Gasification zone; Voxelization method; The Delaunay triangulation approach

1 Introduction

Underground coal gasification (UCG) is a technology used to recover combustible gases such as H_2, CO, and CH_4 by burning coal with gasification agents (air, O_2, water vapor, etc.) delivered through injection wells. This technique is mainly applied in deep coal seams, low coal seams and unworkable coal seams by conventional methods [1-3]. As gasification proceeds, the coal is continuously consumed, and a cavity in the gasification zone will gradually form between the injection and production wells; the volume of this cavity will continue to expand as gasification proceeds, thus causing increased damage to the coal seam, which may lead to a series of problems such as gas leakage, ground subsidence, and groundwater contamination [4-7]. Therefore, it is necessary to monitor cavity expansion in the gasification zone and to estimate the volume change in the gasification zone using an efficient and accurate method.

Scholars from various countries have conducted a series of studies on the monitoring and control of Underground Coal Gasification (UCG). For example, researchers have focused on studying the combustion state in the gasification zone during cavity growth [8-11]. Additionally, many scholars have also investigated other aspects of cavity growth: Perkins et al. modeled the cavity with a packed bed model or as a free channel model, and the form of the channel was mostly considered to be cylindrical or rectangular [12-17]. Samdani et al. predicted the chamber-scale UCG cavity growth rate with an in-house developed computational fluid dynamics (CFD) model and compared it with the data obtained from chamber experiments [18-24]. Mehdi Najaf et al. used multivariate nonlinear regression analysis to establish a new model for predicting the cavity growth rate, which can be used to estimate the cavity growth rate under any given set of parameters [25]. C. Hsu, Blinderman et al. studied the formation of cavities during in situ gasification using the forward combustion linking (FCL) method [26] and determined the shape of the cavities using microfocus X-ray computed tomography [27]. Xiaopeng Liu et al. established a numerical calculation model for the temperature field inside the cavity with varying thermal parameters using the explicit finite difference method. They estimated the diffusion range of temperature inside the combustion cavity [28]. V. Prabu et al. studied the formation of UCG cavities under different experimental conditions and analyzed the results. The findings showed that the shape and formation rate of cavities were significantly affected by the oxygen flow rate, and they also highlighted the importance of ash content in cavity growth [29, 30].

It is important to understand the development of gasification zone cavities to establish safe UCG technology. As the gasification process progresses, the appearance of thermal stresses inside the coal body leads to the generation of cracks, and the locations of these cracks can be detected by acoustic emission (AE) monitoring, making it possible to monitor cavity growth using AE technology. As the cracks expand, the oxidation surface area of the coal seam increases, and combustion and gasification occur in a chain reaction-like manner. Therefore, the combustion and gasification zones will expand and move. In previous studies, AE monitoring technology was used to estimate the evolution of cavities, along with temperature monitoring and analysis of product gas composition. However, there have been few experimental studies that combine the relative energy of AE with the location of AE sources to estimate the expansion of cavities during the entire UCG process.

To achieve the objectives of this study, the stoichiometric method [31,32], the Delaunay triangulation approach [33], and the voxelization method were used to estimate the cavity volume of the gasification zone, and the relationship between coal consumption, gas composition, and temperature distribution was assessed. The stoichiometric method was used to estimate the volume of the gasification cavity by analyzing the gas composition, while the Delaunay triangulation approach and the voxelization method were used to estimate the volume of the gasification cavity by analyzing the AE source information. The stoichiometric method was used to estimate the cavity volume of the gasification zone by calculating the oxygen reaction amount and the carbon content of coal during the UCG process. The formula derivation of this method was based on the conservation of elements in the UCG chemical reaction process. Furthermore, the Delaunay triangulation approach and the voxelization method utilize AE technology as a monitoring tool to estimate the location and magnitude of AE events in the gasification zone by analyzing the waveform of elastic waves caused by thermal stress during the coal gasification process [34]. Based on this, the combustion gasification area of coal can be estimated, and the gasification zone can be visualized. The Delaunay triangulation approach, which takes the Lawson algorithm as its core idea, estimates the gasification cavity volume by constructing a tetrahedral mesh based on the source positions. On the other hand, the voxel method estimates the volume by combining the relationship between the AE source positions and the relative energy. The actual gasification zone cavity volume change was obtained by dividing the coal consumption monitored by electronic mass balance by the apparent density of the coal. The effectiveness of the three methods was verified by comparing and analyzing the estimated volumes obtained from the three methods with the actual change in gasification cavity volume.

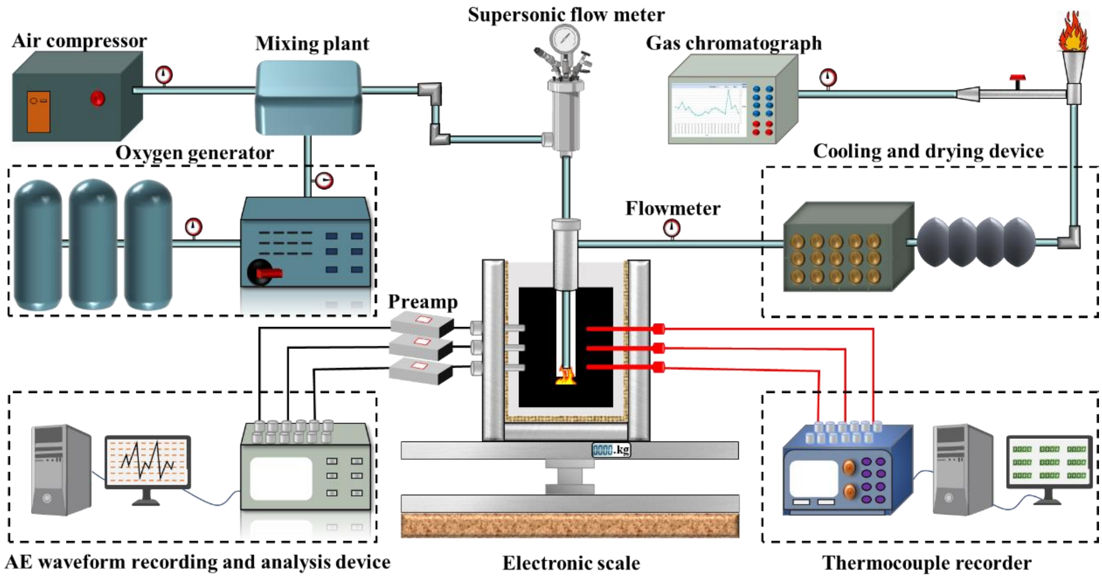

Fig. 1. Experimental system diagram.

2 Materials and methods

2.1 Experimental apparatus

The underground gasification system used in this experiment is shown in Fig. 1. The experiment was conducted using coal blocks. The coal samples were provided by Hokkaido Mining Company, Japan, and the industrial and elemental analyses of the coal samples are shown in Table 1. The whole coal body was cut and put into a sealed iron barrel (Fig. 2 a, b). The length and width of the coal body were controlled at 19~21 cm, the height was 24~26 cm, and refractory cement was poured between the coal body and the iron barrel. The entire underground gasification system was placed on an electronic mass balance, allowing real-time observation of coal mass changes during the gasification process. The gasifying agent was injected using a combination of an air compressor and an oxygen generator, with flow control achieved through the use of a supersonic flowmeter. For this experiment, the cooled product gas was passed through a synthetic gas cooling device before being cooled further and dried in a drying box to remove impurities such as tar. Temperature sensors and AE sensors were installed on both sides of the coal seam to monitor the gasification zone temperature and AE signals, respectively. The cleaned product gas was then fed into a gas chromatograph for analysis.

(a) (b) (c)

Fig. 2. Sensor arrangement, furnace body and output gas for successful ignition. (a) Coal block cutting. (b) Gasification furnace. (c) Successful ignition

Table 1 Industrial and elemental analyses of coal.

Calorific Value (MJ/kg)	Proximate Analysis (wt.%)				Ultimate Analysis (wt.%)				
	Moisture	Ash	Volatiles	Fixed Carbon	C	H	N	S	O
31.48	1.10	8.10	44.90	45.90	75.00	5.78	1.23	0.07	9.71

2.2 Experimental procedure

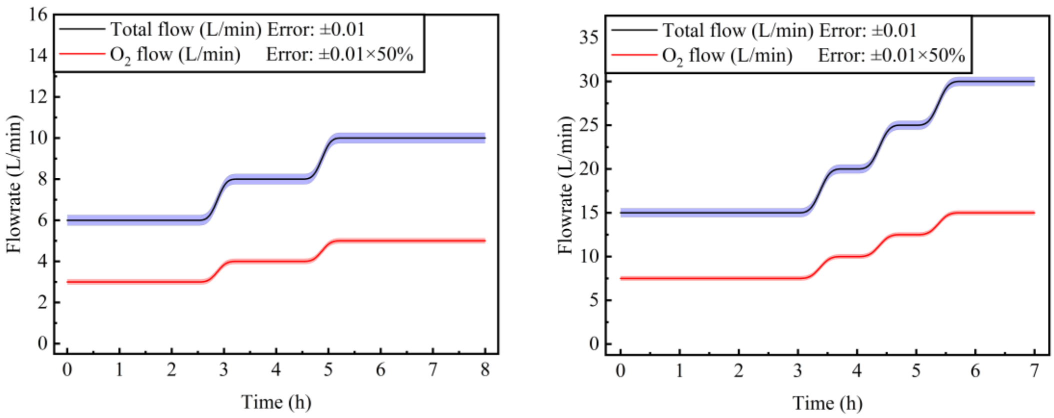

(a) (b)

Fig. 3. Feed gas flow during the gasification experiments. (a) Experiment 1. (b) Experiment 2.

For this experiment, a coaxial tube was used, which consisted of an inner and outer tube. The inner tube was used to inject a mixture of oxygen and air as the gasifying agent, while the outer tube was used to output the product gas after gasification. The distance between the tube opening and the coal bottom was 3 cm, and the diameter of the passage inside the tube was 3 cm. The experiment began by igniting the bottom of the coal with ignition materials such as sawdust, followed by the injection of a mixture of air and oxygen. The experiment used an adsorption-type oxygen making machine (product code: 20D089101) to produce oxygen. The device uses high-quality molecular sieves as adsorbents and utilizes the PSA (PRESSURE SWING ADSORPTION) variable pressure adsorption principle to directly obtain oxygen from compressed air. By mixing with the air output from the air compressor, a mixed gas with a stable oxygen concentration of 50% can be output. The ultrasonic flowmeter used in this experiment employs the principle of time difference propagation. Ultrasonic sensors are installed at two positions, upstream and downstream, to measure the speed of sound propagation from upstream to downstream and from downstream to upstream in order to calculate the fluid flow rate. In addition, the ultrasonic flowmeter includes an integrated thermometer and barometer, which can be used to correct the flow rate and pipe diameter to provide a corrected value output at standard conditions (0 ℃, 1 atm). The minimum measurable flow rate is 0.5 L/min, with a minimum measurable flow rate of 1 L/min when considering the diameter of the pipe used. Due to limitations arising from the precision of the measuring instrument and operational technique, the measurement error of the flow rate is ±0.01 L/min.

Experiment 1 was divided into three stages (1a, 1b, and 1c) based on changes in oxygen flow rate. In stage 1a (0-3 h), the oxygen flow rate was 3 L/min; in stage 1b (3-5 h), it was 4 L/min; and in stage 1c (5-8 h), it was 5 L/min. Experiment 2 was divided into four stages (2a, 2b, 2c, and 2d). In stage 2a (0-3.5 h), the oxygen flow rate was 7.5 L/min; in stage 2b (3.5-4.5 h), it was 10 L/min; in stage 2c (4.5-5.5 h), it was 12.5 L/min; and in stage 2d (5.5-7 h), it was 15 L/min, as shown in Fig. 3. The product gas was cooled and dried to remove tar and other impurities before being analyzed using a gas chromatograph. Gas composition data were recorded every half hour on average. The experiment was ended by extinguishing the fire using N_2.

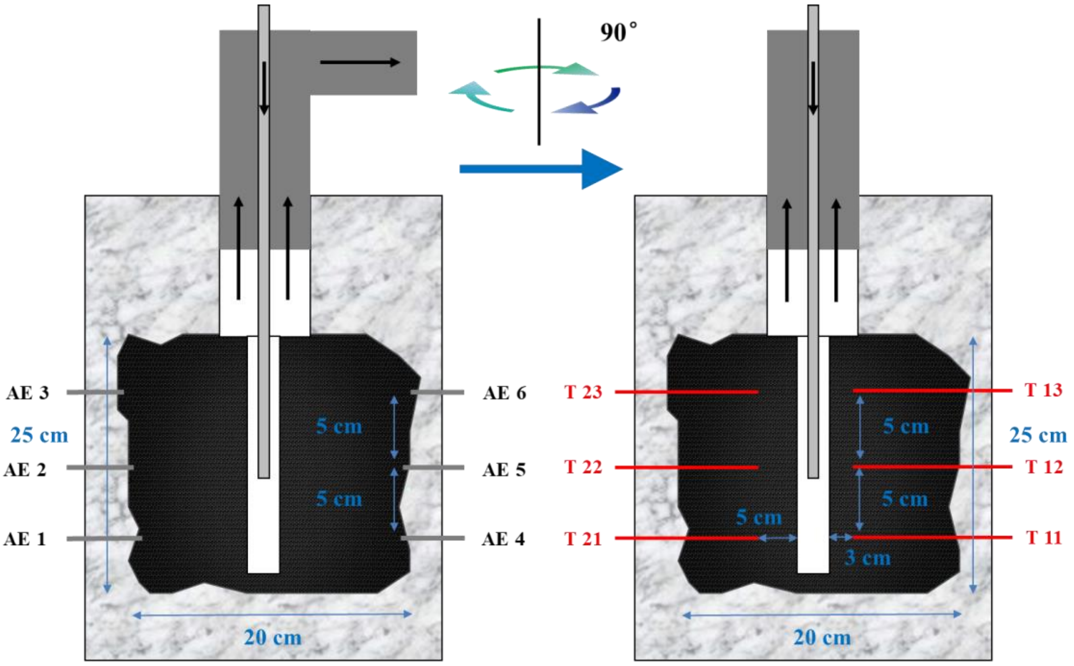

(a) (b)

Fig. 4. Layout of sensors. (a) Piezoelectric acceleration transducers. (b) Thermocouples.

Temperature changes were monitored using K-type thermocouples, which were arranged in layers according to their distance from the ignition point. The first layer, consisting of thermocouples T11 and T21, was placed near the ignition point, and subsequent layers were placed 5 cm apart from each other. The second layer consisted of thermocouples T12 and T22, and the third layer consisted of thermocouples T13 and T23, as shown in Fig. 4. Thermocouples T11-T13 on the right side of the gasification channel were placed closer to the channel at a distance of 3 cm, while thermocouples T21-T23 on the left side were placed farther away at a distance of 5 cm. AE signals were monitored using piezoelectric acceleration sensors. The physical nature of AE is the rapid release of elastic waves due to the local energy of the material. In the process of underground coal gasification, AE activity is mainly caused by thermal stress that leads to coal fracturing. The AE sensors and temperature sensors were arranged perpendicular to each other in terms of their distribution direction. All six AE sensors were inserted into the coal seam at a depth of 1 cm, as shown in Fig. 4. The thermocouples and AE sensors were arranged in the same way for both experiments. In addition, the weight of the gasifier was recorded every half hour using an electronic scale. After the experiment was completed, gypsum slurry was injected into the coal body and allowed to dry. The gasifier was then cut open along the center of the coal body, including the refractory cement.

3 Results and discussion

3.1 Relationship between coal seam temperature distribution and coal consumption

3.1.1 Monitoring of coal consumption by electronic mass balance

The entire underground gasification system was placed on an electronic scale, and the actual coal consumption during stages 1a, 1b, 1c, 2a, 2b, 2c, and 2d was monitored and is shown in Table 2 (calculated dry coal density = 0.92 g/cm^3). Overall, coal consumption in the gasification zone increased significantly with increasing oxygen flow rate, indicating that a higher oxygen flow rate leads to a faster reaction rate. Similar results, where the gasification zone cavity volume significantly increases with increasing oxygen flow rate, have been reported in the literature [30].

Table 2 Coal consumption by stage.

Experiment no.	Stage	Total time (h)	Feed flow rate (L/min)		Oxygen concentration (%)	Time interval (h)	Coal consumption (g)	Coal consumption rate (g/h)	Cavity expansion rate (cm^3/h)
			O_2	Oxygen-enriched air					
1	1a	8	3.0	6	50%	0-3	885.5	295.2	320.8
	1b		4.0	8		3-5	544.9	272.4	296.1
	1c		5.0	10		5-8	936.5	312.2	339.3
2	2a	7	7.5	15	50%	0-3.5	2270.2	648.6	705.0
	2b		10.0	20		3.5-4.5	593.7	593.7	645.3
	2c		12.5	25		4.5-5.5	630.5	630.5	685.4
	2d		15.0	30		5.5-7	1041.6	694.4	754.8

3.1.2 Temperature change

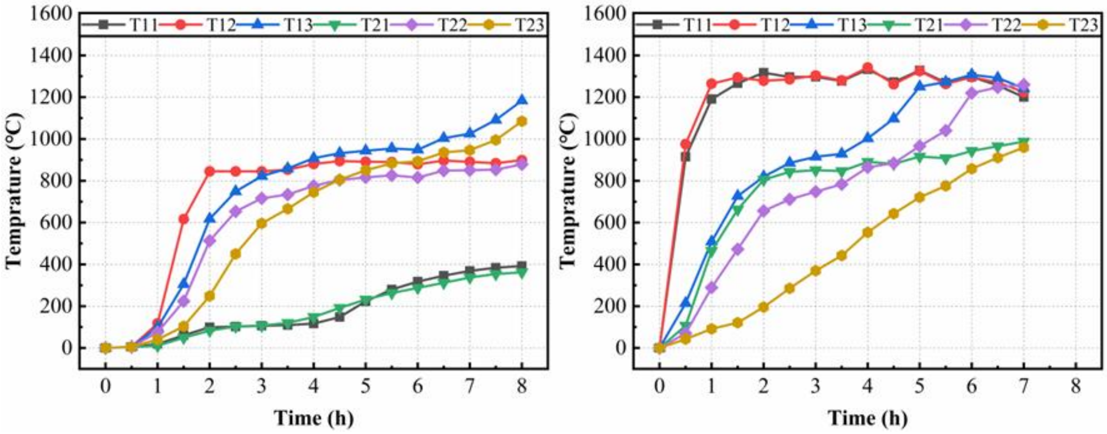

(a) (b)

Fig. 5. Temperature profiles. (a) Experiment 1. (b) Experiment 2.

Fig. 5 shows the temperature variation curves with time during the gasification process. The overall observations indicated that the coal seam temperature rose sharply in the early stage of the experiment, and the rising trend of the coal seam temperature slowed in the middle and late stages of the experiment.

Observations of temperature during experiment 1 revealed that the sharp increase in temperature did not occur at the ignition point (T11), but rather at T12 above the ignition point, where the temperature change was more dramatic than at T11. The temperature rise was particularly apparent near the gas injection port, where T12, T22, T13, and T23 showed a rapid increase, indicating that the gasification zone did not start from the area around the ignition point, but rather from the vicinity of the injection port. This may be due to the effect of the low oxygen flow rate (3 L/min), which caused the oxygen concentration at the ignition point to be lower than that near the injection port. The temperature recorded by T12 rose rapidly to approximately 800℃ at approximately 2 h, while the temperatures recorded by T11 and T21 remained below 200℃. As experiment 1 progressed to approximately 5 h and the oxygen flow rate increased (5 L/min), the temperatures of T13 and T23 above the gasification channel increased more quickly, indicating that the combustion gasification zone was expanding towards the gas outlet direction, as shown in Fig. 5(a).

In experiment 2, the temperature at the ignition point (T11) increased significantly, reaching approximately 1300℃ after approximately 1 h. At the same time, with the injection of a high oxygen flow rate (7.5 L/min), the temperature of T21 at the bottom, far from the gas outlet direction also increased rapidly. This is different from the change in T21 observed in experiment 1. It can be inferred that under high flow rate conditions, the gasification zone first develops downwards from the injection port, then expands to the surrounding upper part, and finally expands outwards along the gas outlet direction, as shown in Fig. 5(b).

3.1.2 Correlation analysis between temperature and coal consumption rate

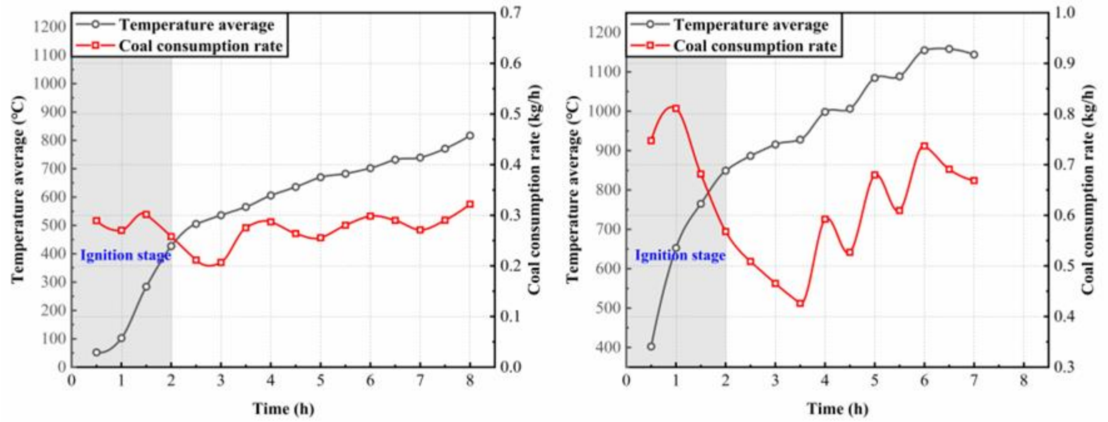

(a) (b)

Fig. 6. Relationship between temperature and coal consumption rate. (a) Experiment 1. (b) Experiment 2.

Fig. 6 shows the curves of the average temperature and coal consumption rate of the gasification zone over time for the two experiments. During the first two hours of both experiments, the gasification zone was in the ignition stage, and the gasification state was unstable. After 2 h, there was a strong correlation between the two parameters, and the coal consumption rate increased with increasing average temperature of the gasification zone. In experiment 1, the coal consumption rate peaked at 0.32 kg/h when the average temperature of the gasification zone reached its highest point of 800.3℃. In experiment 2, the coal consumption rate peaked at 0.74 kg/h when the average temperature of the gasification zone reached its highest point of 1154.8℃. We also found that the coal consumption rate changed dramatically with the changes in temperature, as seen in the period between 3.5 h and 6 h in experiment 2.

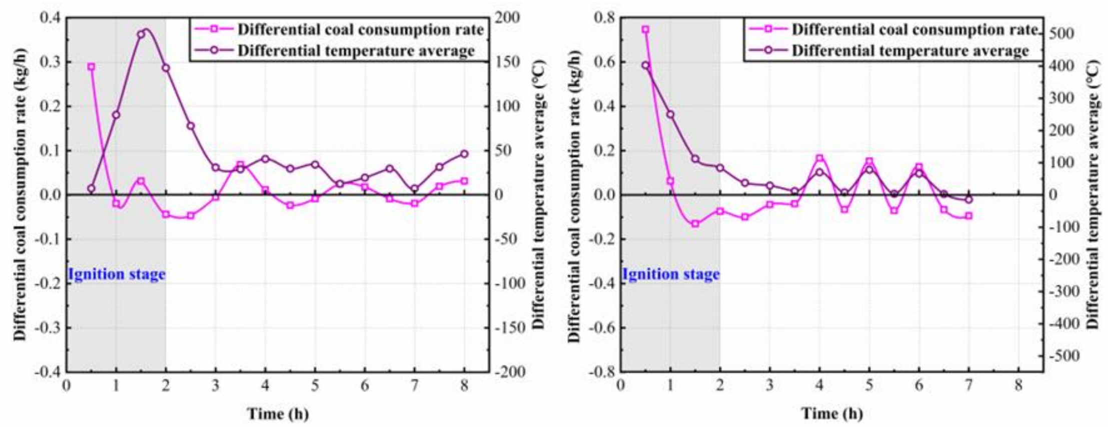

(a) (b)

Fig. 7. Differential average temperature and differential coal consumption rate curves. (a) Experiment 1. (b) Experiment 2.

By using the first-order forward difference method to analyze the coal consumption rate and average temperature data of experiments 1 and 2, we obtained Fig. 7, where the differential coal consumption rate represents the overall change in the gasification zone coal consumption rate between two adjacent time points, and the differential average temperature represents the overall change in the gasification zone temperature between two adjacent time points. From the overall trend, there is a strong correlation between the differential average temperature and the differential coal consumption rate, which is particularly evident in experiment 2. As experiment 2 progressed from stages 2a, 2b, and 2c to stages 2b, 2c, and 2d, the difference in average temperature increased by 58.4℃, 70.3℃, and 62.6℃, respectively, while the difference in coal consumption rate increased by 0.21 kg/h, 0.22 kg/h, and 0.20 kg/h. With the rapid changes in oxygen flow rate, the difference in average temperature also changed rapidly, and the difference in coal consumption rate showed the same trend as the difference in average temperature, as shown in Fig. 7(b).

3.2 Estimation of cavity growth in the gasification zone by gas composition

3.2.1 Product gas composition

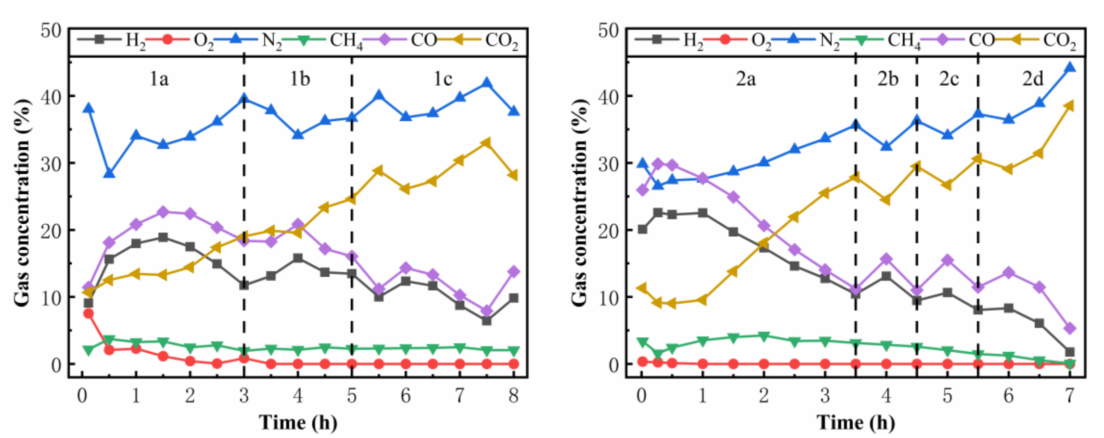

(a) (b)

Fig. 8. Composition of the gas generated during gasification. (a) Experiment 1. (b) Experiment 2.

By comparing the concentrations of CO and H_2 in the product gas at three stages of experiment 1 and four stages of experiment 2, we found that the changes in CO and H_2 concentrations were closely related to the oxygen flow rate. In stage 1a of experiment 1, the gasification zone reaction state was unstable. In stage 1b, with increases in the oxygen flow rate and in the internal temperature of the coal, there was a significant increase in CO and H_2 concentrations. After further increasing the oxygen flow rate and entering stage 1c, the concentrations of CO and H_2 showed a decreasing trend. Overall, in experiment 2, the oxygen flow rate was too high, and the concentrations of CO and H_2 in the product gas showed a decreasing trend.

3.2.2 Volume estimation based on stoichiometry

Stoichiometry was used to estimate the UCG gasification process, and the chemical reactions during the underground gasification process were represented by the elemental balance equation given in Equation (1), where H_2, CO, CO_2 and CH_4 are the main components of the dry gas, and their concentrations in the generated gas are represented by p, q, r, and s, respectively. The values of m and n were obtained through the elemental analysis of the coal sample, while α and β represent the equilibrium constants of O_2 and H_2O, respectively. γ, δ, ε, and η represent the gas yields of H_2, CO, CO_2 and CH_4, respectively.

$$CH_mO_n + \alpha O_2 + \beta H_2O \rightarrow \gamma H_2 + \sigma CO + \varepsilon CO_2 + \eta CH_4 \quad (1)$$

The gas composition of the main product gases and the stoichiometrically estimated coal consumption at different oxygen flow rates are presented in Table 3.

Table 3 Gas concentrations and coal consumption at different oxygen flow rates.

Stage	O_2 (%)	N_2 (%)	CO_2 (%)	CO (%)	CH_4 (%)	H_2 (%)	Coal consumption (g)
1a	2.3	34.04	13.43	20.80	3.27	17.96	832.1
1b	0.0	34.10	19.57	20.90	2.11	15.78	523.0
1c	0.0	36.78	26.14	14.30	2.36	12.35	889.9
2a	0.0	28.71	13.81	24.91	4.01	19.70	2133.9
2b	0.0	32.37	24.51	15.66	2.86	13.10	569.6
2c	0.0	34.09	26.71	15.48	2.06	10.64	604.1
2d	0.0	36.43	29.11	13.65	1.25	8.32	994.7

Table 4 compares the estimated cavity volume of the gasification zone obtained by stoichiometry and the actual cavity volume of the gasification zone at each stage. Due to the unstable gasification situation in the early stage of the experiment, the estimation errors of stages 1a and 2a were 6.04% and 6.0%, respectively, while the estimation errors of the other stages were all less than 5%. The best stage for estimation was stage 1b, with an estimation error of 4.01%. Overall, in experiment 1, the actual cavity volume of the gasification zone was 2572.7 cm^3, and the estimated total volume was 2440.1 cm^3, which was 5.2% smaller than the actual volume. In experiment 2, the actual cavity volume of the gasification zone was 4930.5 cm^3, and the estimated total volume was 4332 cm^3, which was 5.1% smaller than the actual volume. These results indicate that this theory can be used to estimate the gasification chamber volume accurately.

Table 4 Changes in the estimated volume by stoichiometry and the actual cavity volume of the gasification zone.

Stage	1a	1b	1c	2a	2b	2c	2d
Cavity volume by stoichiometric method (cm^3)	904.3	568.5	967.3	2319.5	619.1	656.6	1081.2
Actual cavity volume (cm^3)	962.5	592.2	1017.9	2467.6	645.3	685.4	1132.2
Error (%)	6.04	4.01	4.98	6.00	4.06	4.20	4.50

3.3 Estimation of cavity growth in the gasification zone by AE

3.3.1 AE source location calibration

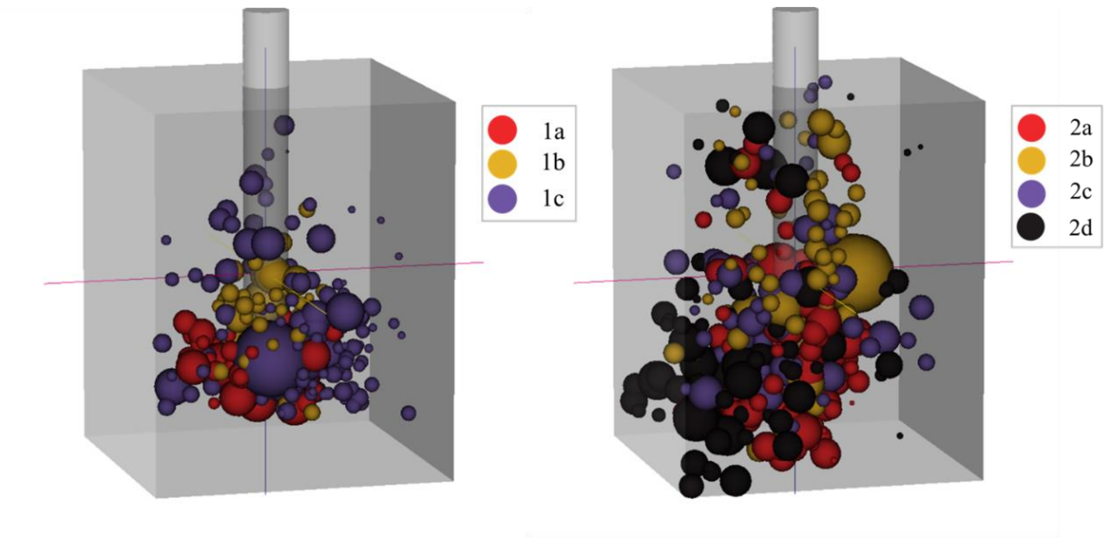

(a) (b)

Fig. 9. Results of AE source location. (a) Experiment 1. (b) Experiment 2.

The AE source location calibration results were obtained by applying the least-squares iterative algorithm [35], as shown in Fig. 9. The location of the AE source was calculated by combining the arrival time of the primary wave and the coordinates of each AE sensor. The center of the sphere represents the location of the source, and the AE events generated during different oxygen flow rate stages were divided into different phases. Experiment 1 was divided into three stages, namely, 1a, 1b, and 1c, while experiment 2 was divided into four stages, namely, 2a, 2b, 2c, and 2d. Different colors were assigned to different stages, and the size of the spheres represents the relative energy. The degree of extension of the coal seam fractures during the gasification process can be represented by the relative energy of AE, denoted as A_e, which is calculated as the square of the range of AE source energy A_0, according to Equation (2).

$$A_0 = \frac{1}{N}\sum_{j=1}^{N}(A_j \times L_j) \qquad A_e = (A_0)^2 \tag{2}$$

Here, L_j represents the distance between the calibration location of the AE source and the jth AE sensor, N is the number of AE sensors, and A_j is the maximum amplitude of the waveform obtained from the jth AE sensor.

In both experiments, the majority of the AE sources were concentrated around the coaxial hole and moved upward with time. During stages 1a and 2a, the AE sources were mainly distributed at the gas injection port and the ignition point, indicating that the fracture activity was most intense during these two stages and more cracks appeared. During stages 1b, 1c, 2b, 2c, and 2d, the fractured area mainly evolved from the gas injection port to the top gas outlet. Compared to experiment 1, experiment 2 had a larger number of large-scale AEs caused by the high oxygen flow rate, and during stage 2b, the AE sources began to spread upward in large numbers. During stages 2c and 2d, the AE sources spread to the edge of the coal seam. This phenomenon indicated that gasification started from the ignition point and gradually moved outward and upward, and high oxygen flow rates caused AE sources to spread upward more quickly.

3.3.2 Volume estimation based on the Delaunay triangulation approach

To study the cavity volume in the gasification zone, the Delaunay triangulation method was used based on the results of AE source positioning. This method is a geometric technique of combining given point source data into triangles. In this method, the circumcircle of each triangle does not contain any other point source data, so the triangles formed by each division are closest to equilateral triangles. The Delaunay triangulation method is widely used as an automatic element division method [33] in various numerical simulation software programs.

The process of 2D Delaunay triangulation began by creating a super triangle that contains all the source points and then inserting the concentrated source point data one by one. The triangle whose circumcircle contains the inserted point is called the influence triangle of that point. The common edges of the influence triangles were removed, and the inserted point was connected to all the vertices of the triangles to complete the insertion of the source data into the Delaunay triangulation data set. This process was repeated until no more points needed to be added. This step was then extended to 3D. Then, a sphere was created that contains all the source points. The maximum and minimum points of the X, Y, and Z axes in the source point data were found, and the center coordinates of each axis were calculated. When the maximum values are maxX, maxY, and maxZ and the minimum values are minX, minY, and minZ, the center coordinates centerX, centerY, and centerZ for each axis are given by Equation (3).

$$centerX = \frac{1}{2}(maxX + minX)$$

$$centerY = \frac{1}{2}(maxY + minY)$$

$$centerZ = \frac{1}{2}(maxZ + minZ) \tag{3}$$

Then, the radius was calculated using Equation (4), and by adding 0.1 to the radius, a new radius r that contained all the source point data was obtained.

$$r = \sqrt{(centerX - minX)^2 + (centerY - minY)^2 + (centerZ - minZ)^2} + 0.1 \tag{4}$$

The coordinates of the four points of the circumscribed tetrahedron, P1, P2, P3, and P4, were obtained using the center coordinates of the axis and the radius r. The coordinates of P1, P2, P3, and P4 are given by Equation (5):

$$P_1(x_{1,}\, y_{1,}\, z_{1,}) = (centerX,\quad 3r,\quad centerZ)$$

$$P_2(x_{2,}\, y_{2,}\, z_{2,}) = \left(centerX - 2r\sqrt{2},\quad centerY - r,\quad centerZ\right)$$

$$P_3(x_{3,}\, y_3\, z_{3,}) = \left(centerX + r\sqrt{2},\quad centerY - r,\quad centerZ + r\sqrt{6}\right)$$

$$P_4(x_{4,}\, y_{4,}\, z_{4,}) = \left(centerX + r\sqrt{2},\quad centerY - r,\quad centerZ - r\sqrt{6}\right) \tag{5}$$

Finally, the concentrated source point data were inserted one by one using a method called incremental insertion. Fig. 10 shows the tetrahedral division performed by the incremental insertion method. To determine if an inserted point was contained within the circumscribed sphere of the tetrahedron, the center coordinates O (x_0, y_0, z_0) and radius R of the circumscribed sphere were obtained using Equations (7) and (8). If the inserted source point was located inside the circumscribed sphere of the tetrahedron, the common edges of the tetrahedron were removed, and the inserted point was connected to all the vertices of the tetrahedron. This process of tetrahedral division was repeated until no more points needed to be added.

$$V = 1/6 \left\| \begin{matrix} x_2 - x_1 & y_2 - y_1 & z_2 - z_1 \\ x_3 - x_1 & y_3 - y_1 & z_3 - z_1 \\ x_4 - x_1 & y_4 - y_1 & z_4 - z_1 \end{matrix} \right\| \tag{6}$$

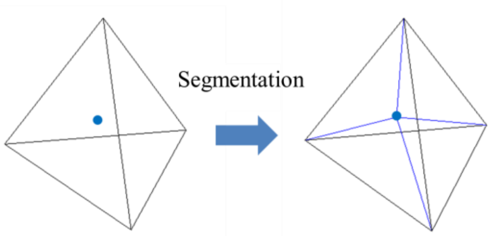

Fig. 10. The incremental insertion method was used to perform tetrahedral division.

$$x_0 = 1/120V^2 \begin{vmatrix} x_1^2 + y_1^2 + z_1^2 & y_1 & z_1 & 1 \\ x_2^2 + y_2^2 + z_2^2 & y_2 & z_2 & 1 \\ x_3^2 + y_3^2 + z_3^2 & y_3 & z_3 & 1 \\ x_4^2 + y_4^2 + z_4^2 & y_4 & z_4 & 1 \end{vmatrix}$$

$$y_0 = 1/120V^2 \begin{vmatrix} x_1^2 + y_1^2 + z_1^2 & x_1 & z_1 & 1 \\ x_2^2 + y_2^2 + z_2^2 & x_2 & z_2 & 1 \\ x_3^2 + y_3^2 + z_3^2 & x_3 & z_3 & 1 \\ x_4^2 + y_4^2 + z_4^2 & x_4 & z_4 & 1 \end{vmatrix}$$

$$z_0 = 1/120V^2 \begin{vmatrix} x_1^2 + y_1^2 + z_1^2 & x_1 & y_1 & 1 \\ x_2^2 + y_2^2 + z_2^2 & x_2 & y_2 & 1 \\ x_3^2 + y_3^2 + z_3^2 & x_3 & y_3 & 1 \\ x_4^2 + y_4^2 + z_4^2 & x_4 & y_4 & 1 \end{vmatrix} \tag{7}$$

$$R = \sqrt{(x - x_i)^2 + (y - y_i)^2 + (z - z_i)^2} \; (i = 1, 2.3, 4) \tag{8}$$

The Delaunay triangulation approach did not consider the weights of points, and it was necessary to preprocess the point cloud data. AE data with relative energy below 0.001 were regarded as small cracks and excluded, and AE data outside the coal body beyond a certain distance from the centroid of the AE source distribution was also excluded [34]. The processed AE source point cloud data were used to construct a three-dimensional tetrahedral mesh model. The basic unit of the Delaunay triangulation process was a tetrahedron, and its volume could be obtained using Equation (8). Based on the results of experiment one and experiment two, the estimated and actual changes in cavity volume of the gasification zone at various flow rates are summarized in Table 5.

Table 5 The changes in the estimated volume obtained by the Delaunay triangulation approach and the actual cavity volume of the gasification zone.

Stage	1a	1b	1c	2a	2b	2c	2d
Cavity volume determined by the Delaunay triangulation approach (cm^3)	1048.1	663.3	1252.0	2862.4	695.6	748.4	1381.2
Actual cavity volume (cm^3)	962.5	592.2	1017.9	2467.6	645.3	685.4	1132.2
Error (%)	8.90	12.00	23.00	16.00	7.80	9.20	22.00

The shapes of the cavity of the gasification zone obtained by the Delaunay triangulation approach are shown in Figs. 11 and 12. Subfigures 1a, 1b, and 1c represent the results of experiment one at 0-3 h, 0-5 h, and 0-8 h, respectively. Subfigures 2a, 2b, 2c, and 2d represent the results of experiment two at 0-3.5 h, 0-4.5 h, 0-5.5 h, and 0-7 h, respectively. As shown in Table 5, the estimation errors were all less than 25%, with a minimum of 7.8% during stage 2b. The maximum estimation error of 23% occurred during stage 1c. The reason for the estimation error may be that this method cannot describe nonconvex regions. Therefore, if the combustion zone contains nonconvex regions, this method may include them in the gasification zone, resulting in overestimation of the cavity volume and coal consumption in the gasification zone.

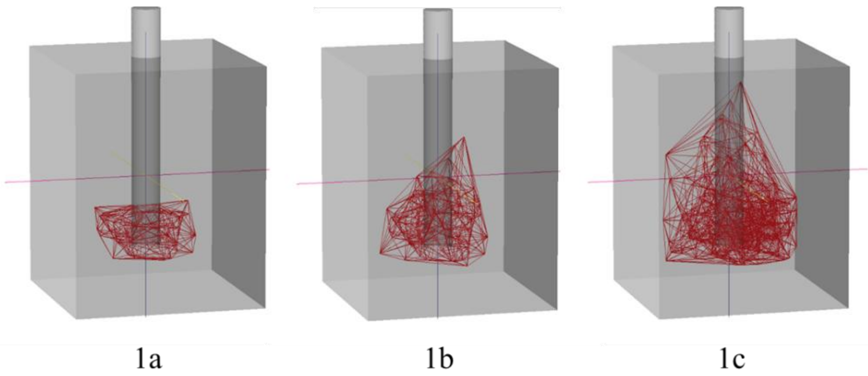

Fig. 11. Results of Delaunay triangulation to estimate the cavity of the gasification zone (Experiment 1). (1a) 0-3 h cavity effect. (1b) 0-5 h cavity effect. (1c) 0-8 h cavity effect.

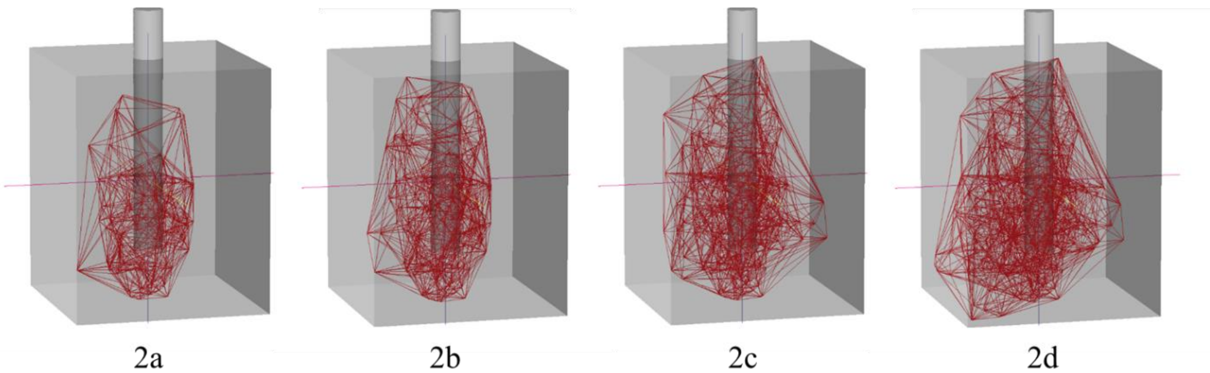

Fig. 12. Results of Delaunay triangulation to estimate the cavity of the gasification zone (Experiment 2). (2a) 0-3.5 h cavity effect. (2b) 0-4.5 h cavity effect. (2c) 0-5.5 h cavity effect. (2d) 0-7 h cavity effect.

3.3.3 Volume estimation based on the Delaunay triangulation approach

Due to the limitations of the Delaunay triangulation approach in estimating the cavity volume of the gasification zone and its inability to describe nonconvex regions, the point cloud data used in this study considered only the AE source point coordinates and did not consider other AE data. To minimize errors, a voxel-based method was proposed for volume evaluation. This method can describe nonconvex regions and considers the relative energy of AE as the weight of the point. Voxels with a size corresponding to the relative energy of AE were assigned to the source points to represent the cavity volume of the gasification zone.

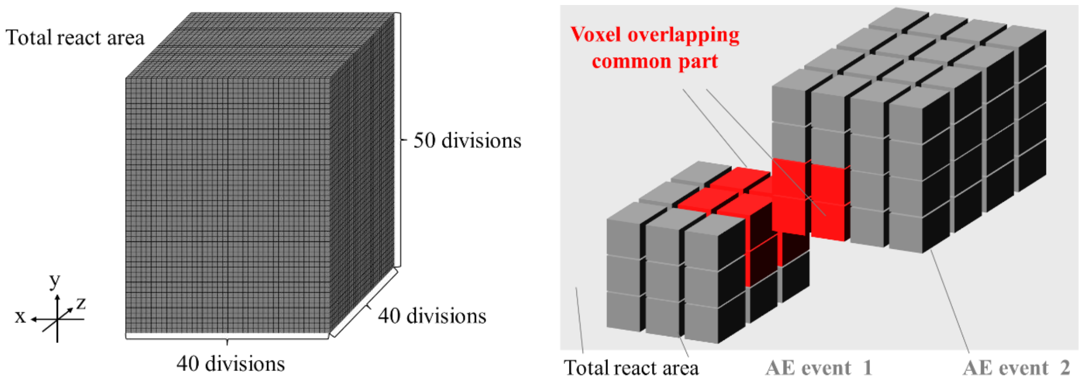

(a) (b)

Fig. 13. Voxel representation method. (a) 3D mesh segmentation of the coal body. (b) Overlap of voxels.

In the voxelization method, the coal body was divided into a three-dimensional grid with 40 divisions in the x and z directions and 50 divisions in the y direction, creating a total of 40 × 40 × 50 cubes, as shown in Fig. 13(a). Each cube is called a voxel, and each voxel was assigned a volume of 0.125 cm^3 (the original coal body was 20 × 20 × 25 cm^3, and each voxel's volume is equivalent to 1/80,000 of the original coal body). Based on the relative energy of AE within a certain range, values were input into the voxels, as shown in Fig. 13(b), which displays the data for two different AE source points with energy sizes of 3 × 3 × 3 and 4 × 4 × 4 voxels. The common portion of the two source points is the overlapping section (2 × 2 × 2 voxels), and the advantage of this method is that the overlapping section is not double-counted when assigning values to the voxels. This method can accurately estimate the cavity volume in the gasification zone, thereby accurately estimating the coal consumption. The sum of the values input into the voxels was used as the volume of the reactive coal.

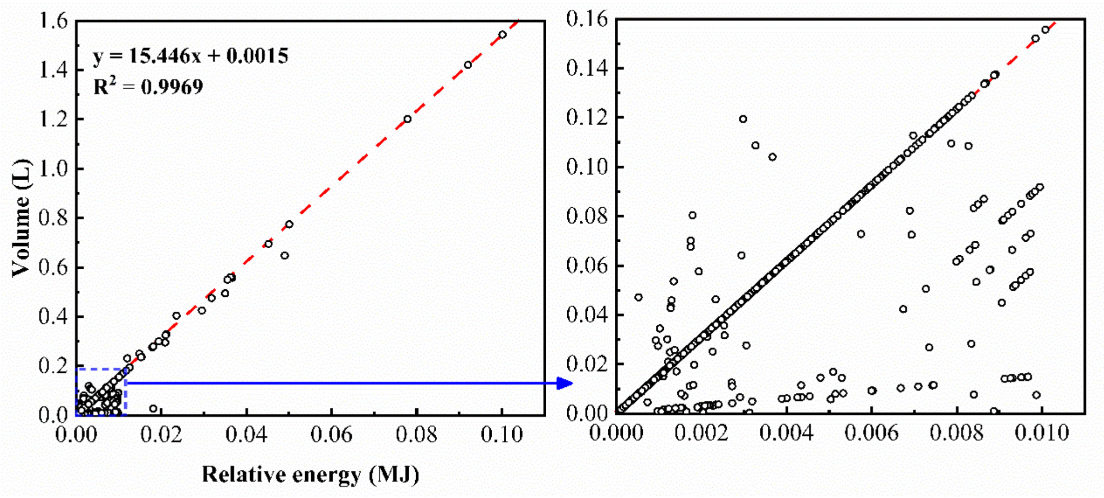

(a) (b)

Fig. 14. (a) Relative energy vs. volume. (b) Relative energy vs. volume. (Relative energy is below 0.011)

In this method, the relative energy data of the AE source points and the actual gasification zone volume data from the two experiments were analyzed and compared. It was found that the relationship between the two data sets was well described by a linear function. Thus, a linear regression was performed to derive an empirical formula that related the actual cavity volume in the gasification zone to the relative energy of the AE source points. The relative energy of the AE source points and the estimated volume were linearly correlated with a correlation coefficient of 0.996, as shown in Fig. 14.

Fig. 14 shows that the data points with relative energy values below 0.011 were more scattered than those with relative energy values above 0.011. Therefore, an error analysis was performed separately for the data points with relative energy values below 0.011. The points that deviated from the fitting curve corresponded to 7.8% of the total number of AE events, and the associated volume accounted for 9.6% of the total volume corresponding to all AE events with relative energy values below 0.011. In terms of the total number of events, the points that deviated from the fitting curve corresponded to 7.2% of the total number of AE events, and the associated volume accounted for 4.1% of the total volume corresponding to all AE events.

Using the empirical formula obtained from Fig. 14, the cavity volume changes in the gasification zone at various oxygen flow rates in the two experiments were estimated. The voxel-based method was used to estimate the cavity volume changes at each flow rate, and the results were compared with the actual cavity volume changes, as shown in Table 6. The estimation error was the smallest during stage 2d, with a maximum error of 4.0%. The maximum error of stage 2a was 10.1%, and the errors in each stage were less than 11%, indicating that the AE source point position information combined with the relative energy can indeed accurately estimate the cavity volume of the gasification zone.

Table 6 The changes in the estimated volume obtained by the voxelization method and the actual cavity volume of the gasification zone.

Stage	1a	1b	1c	2a	2b	2c	2d
Cavity volume by the voxelization method (cm^3)	1022.1	634.9	1081.0	2716.8	684.0	716.2	1177.4
Actual cavity volume (cm^3)	962.5	592.2	1017.9	2467.6	645.3	685.4	1132.2
Error (%)	6.20	7.20	6.20	10.10	6.00	4.50	4.00

The morphology of the gasification zone obtained by the voxelization method is shown in Figs. 15 and 16. Subfigures 1a, 1b, and 1c represent the voxel results for experiment 1 at 0-3 h, 0-5 h, and 0-8 h, respectively. Subfigures 2a, 2b, 2c, and 2d represent the voxel results for experiment 2 at 0-3.5 h, 0-4.5 h, 0-5.5 h, and 0-7 h, respectively.

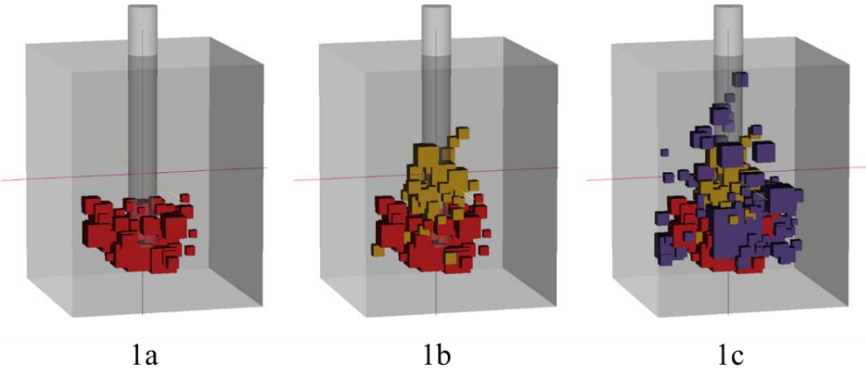

Fig. 15. Results of the voxelization method to estimate the cavity of the gasification zone (Experiment 1). (1a) 0-3 h cavity effect. (1b) 0-5 h cavity effect. (1c) 0-8 h cavity effect.

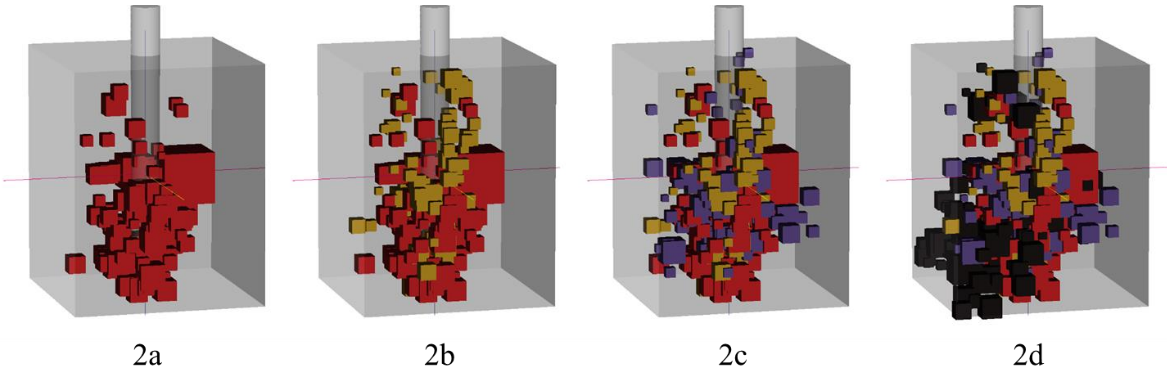

Fig. 16. Results of the voxelization method to estimate the cavity of the gasification zone (Experiment 2). (2a) 0-3.5 h cavity effect. (2b) 0-4.5 h cavity effect. (2c) 0-5.5 h cavity effect. (2d) 0-7 h cavity effect.

3.3.4 Model Errors and Limitations

In summary, the chemical stoichiometry method, Delaunay triangulation method, voxel method, and weighing method are used to calculate the expansion velocity of the gasification cavity. The limitations of the chemical stoichiometry method include the lack of consideration for tar filtered by the filtration system and volatile substances present during the gasification process. As shown in Figure 17(a), this estimation method generally underestimates the expansion velocity of the cavity, with a maximum estimation error of 6.04% in Stage 1a and a minimum estimation error of 4.01% in Stage 1b. Furthermore, the chemical stoichiometry method cannot estimate the shape of the gasification cavity.

As for limitations, the Delaunay triangulation method is not suitable for nonconvex sets. Nonconvex sets have complex topological structures in their boundary regions, making it impossible to establish a continuous and reasonable triangular mesh through nearest neighbour relationships. It may also generate triangles with extreme shapes, leading to overestimated results. As shown in Figure 17(b), this method generally overestimates the expansion velocity of the cavity, with a maximum estimation error of 23% in Stage 1c and a minimum estimation error of 7.8% in Stage 2b.

The limitation of the voxel method lies in the fact that the size of the voxels affects the accuracy and resolution of the estimation results. If the voxels are too large, they cannot accurately describe the detailed structures within the cavity, resulting in inaccurate estimation results. If the voxels are too small, the computational complexity and storage requirements will increase. As shown in Figure 17(c), this method generally overestimates the expansion velocity of the cavity, with a maximum estimation error of 10.1% in Stage 2a and a minimum estimation error of 4.0% in Stage 2d. Additionally, both the voxel method and triangulation method are greatly influenced by the accuracy of acoustic emission for rupture monitoring rather than the algorithms themselves. Improving the accuracy of acoustic emission for rupture monitoring will effectively enhance the accuracy of these two prediction models.

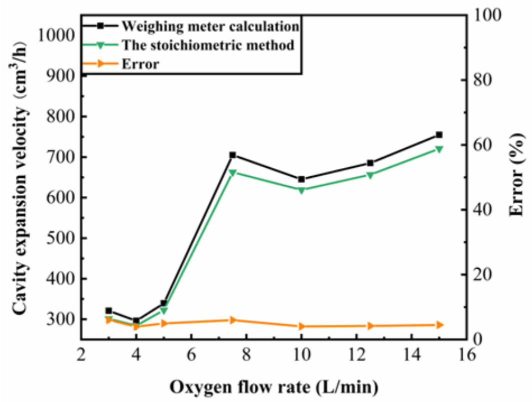

(a)

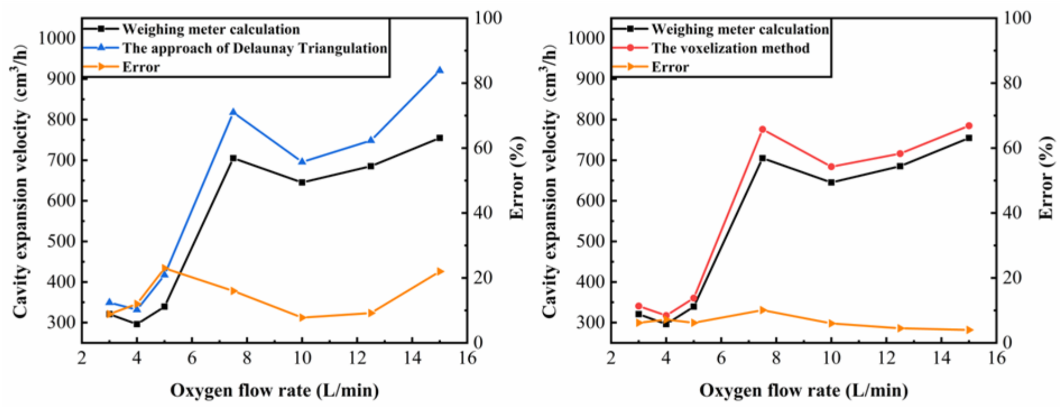

(b) (c)

Fig. 17. The actual value of cavity expansion rate and the estimated value of the gasification zone. (a) The stoichiometric method (b) The Delaunay triangulation approach (c) The voxelization method

After the experiment, we cut the coal sample along the center and compared the profiles obtained by the Delaunay triangulation approach and the voxelization methods, as shown in Fig. 18. The typical nonconvex areas are highlighted using yellow circles. For experiment 1, the voxelization method had an estimation error of 6.4% for the cavity volume in the gasification zone at the end of the experiment, while the Delaunay triangulation approach had an error of 15.2%. Therefore, the voxelization method was 8.8% more accurate than the Delaunay triangulation approach. For experiment 2, the voxelization method had an estimation error of 7.4%, while the Delaunay triangulation approach had an error of 15.4%. Therefore, the voxelization method was 8% more accurate than the Delaunay triangulation approach. From the profiles of the areas numbered 1-3 in the figure, it can be seen that the voxelization method has advantages in estimating the cavity volume of the gasification zone and describing the shape of the cavity and can better address the problems of the Delaunay triangulation approach in overestimating the volume due to inaccurate shape description of nonconvex areas. Finally, the error calculated by overlapping the profile with the triangulation image and the voxelized image is shown in Table 7. It is found that the estimation of section area by triangulation method is closer to the original section area. The reason we speculate here is that the original section actually contains a portion of the unvaporized area, which would be accounted for by triangulation, but not by voxel. In the future, we will consider improving the grouting material and filling the cavity with more suitable materials to ensure higher accuracy.

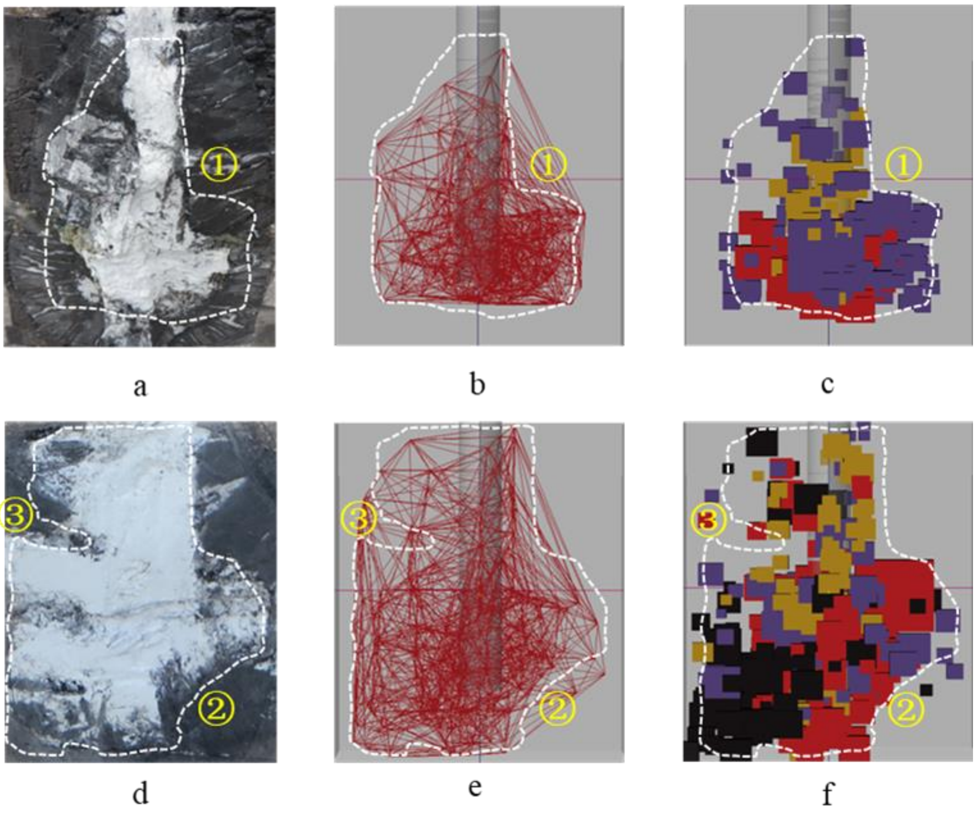

Fig. 18. (a) Actual profile (Experiment 1). (b) Profile obtained by the Delaunay triangulation approach (Experiment 1). (c) Profile obtained by the voxelization method (Experiment 1). (d) Actual profile (Experiment 2). (e) Profile obtained by the Delaunay triangulation approach. (Experiment 2). (f) Profile obtained by the voxelization method (Experiment 2).

Table 7 To compare the section area obtained through voxelization and triangulation with the section area obtained from actual cutting.

Section type	Experiment 1	Experiment 2
Section area by the Delaunay triangulation approach (cm^2)	246.00	396.90
Section area by the voxelization method (cm^2)	236.10	350.52
Actual section area (cm^2)	267.06	397.74
Error (the Delaunay triangulation approach) (%)	-7.89	-0.21
Error (the voxelization method) (%)	-11.59	-11.87

4. Conclusion

(1) The oxygen flow rate in the gasification agent is one of the main factors affecting the coal consumption rate in gasification. Overall, as the oxygen flow rate increases, the coal consumption rate significantly increases. Specifically, when the oxygen flow rate increased from 3 L/min to 15 L/min, the coal consumption rate increased from 295.2 g/h to 694.4 g/h. Moreover, there is a strong correlation between the differential average temperature and differential coal consumption rate. With drastic changes in oxygen flow rate, the differential average temperature quickly changes, and the differential coal consumption rate shows the same trend as the differential average temperature.

(2) AE monitoring combined with Delaunay triangulation is a useful means of visualizing the three-dimensional gasification zone. As the number of AE sources increases, the Delaunay triangulation approach can estimate the shape of the gasification zone in different flow rate stages in real time. The combination of AE monitoring and the Delaunay triangulation approach has good performance in estimating the cavity volume of the convex gasification zone. Specifically, when the oxygen flow rate is 3 L/min, the estimation error is 8.9%, and when the oxygen flow rate is 10 L/min, the estimation error is 7.8%. According to past underground gasification experiments, a convex gasification zone is generally formed under good experimental conditions. Therefore, this method is suitable for estimating the volume of the convex gasification zone.

(3) Compared with the Delaunay triangulation approach, the voxelization method is more effective in estimating the cavity volume of the gasification zone and describing the cavity shape. In terms of estimating the cavity volume of the gasification zone, in experiment 1, the voxelization method had an error of 6.4% after the experiment was completed, while the Delaunay triangulation approach had an error of 15.2%. The voxelization method improved the accuracy by 8.8% compared to the Delaunay triangulation approach. In experiment 2, the voxelization method had an error of 7.4% after the experiment was completed, while the Delaunay triangulation approach had an error of 15.4%. The voxelization method improved the accuracy by 8% compared to the Delaunay triangulation approach. From the comparison of the gypsum profiles in the later stage of the experiment, the voxelization method can describe the cavity shape more accurately.

(4) The stoichiometric method, the Delaunay triangulation approach, and the voxelization method each have their own advantages and disadvantages. The stoichiometric method has good overall

performance in estimating the cavity volume, with small errors, but it cannot describe the three-dimensional shape of the gasification zone. The Delaunay triangulation approach is suitable for evaluating the cavity of the convex gasification zone. The voxelization method can provide a more accurate estimation of the cavity volume and the three-dimensional shape of the gasification zone based on an empirical relationship supported by preliminary experimental data for a specific type of underground gasification experiment. The three methods can be used in combination to effectively and accurately estimate the changes in the cavity of the gasification zone.

Credit author statement

Fa-qiang Su.: Investigation, Writing-Reviewing and Editing, Funding acquisition. Xiao-long He: Investigation, Writing-Original draft preparation, Funding acquisition. Meng-jia Dai: Supervision, Validation. Jun-nan Yang: Investigation, Data curation. Akihiro Hamanaka: Conceptualization, Methodology. Yi-he Yu: Investigation, Validation, Data curation, Funding acquisition. Wen-Li: Investigation, Validation. Jiao-yuan Li: Validation, Resources.

Declaration of Competing Interest

The authors declare that they have no known competing financial interests or personal relationships that could have appeared to influence the work reported in this paper.

Data availability

Data will be made available on request.

Acknowledgments

This work was supported by Key Laboratory of Western Mine Exploitation and Hazard Prevention, Ministry of Education (SKLCRKF1902), State Key Laboratory for Geomechanics and Deep Underground Engineering, China University of Mining & Technology (SKLGDUEK2004), Key R & D and promotion projects (scientific and technological breakthrough) in Henan Province (16220043), Key Scientific Research Project of Colleges and Universities in Henan Province (22B440003), Natural Science Foundation of Henan Province of China (232300421205). The authors gratefully acknowledge their support, and expresses particular appreciation to UCG project members.

References:

[1] Olateju, B. and A. Kumar, Techno-economic assessment of hydrogen production from underground coal gasification (UCG) in Western Canada with carbon capture and sequestration (CCS) for upgrading bitumen from oil sands. Applied Energy, 2013. 111(10): p. 428-440. https://doi.org/10.1016/j.apenergy.2013.05.014

[2] Prabu, V. and S. Jayanti, Underground coal-air gasification based solid oxide fuel cell system. Applied Energy, 2012. 94: p. 406-414. https://doi.org/10.1016/j.apenergy.2012.01.040

[3] Bhutto, A.W., A.A. Bazmi and G. Zahedi, Underground coal gasification: From fundamentals to applications. Progress in Energy and Combustion Science, 2013. 39(1): p. 189-214. https://doi.org/10.1016/j.pecs.2012.09.004

[4] A C L , A H C , B C J ,et al.A back analysis of the temperature field in the combustion volume space during underground coal gasification[J]. 2011, 21(4):5.DOI:10.1016/j.mstc.2011.06.018.

[5] Mallett CW. Environmental controls for underground coal gasification. Proc IMechE Part A: J Power & Energy 2017. https://doi: 10.1177/0957650917723733.

[6] Derbin Y, Walker J, Wanatowski D, Marshall A. Soviet experience of underground coal gasification focusing on surface subsidence. J Zejiang Univ 2015;16:839–50. https://doi: 10.1631/jzus.A1500013.

[7] Mehdi, Najafi Seyed, et al. Prediction of cavity growth rate during underground coal gasification using multiple regression analysis[J]. Int J Coal Sci Technol 2015; 2(4):318–24. https://doi.org/10.1007/s40789-015-0095-9

[8] Khan, M.M.; Mmbaga, J.P.; Shirazi, A.S.; Trivedi, J.; Liu, Q.; Gupta, R. Modelling Underground Coal Gasification—A Review. Energies 2015, 8, 12603–12668. https://doi.org/10.3390/en81112331

[9] Nourozieh, H.; Kariznovi, M.; Chen, Z.; Abedi, J. Simulation Study of Underground Coal Gasification in Alberta Reservoirs: Geological Structure and Process Modeling. Energy Fuels 2010, 24, 3540–3550. https://doi.org/10.1021/ef9013828

[10] Cui, Y.; Liang, J.; Wang, Z.; Zhang, X.; Fan, C.; Liang, D.; Wang, X. Forward and reverse combustion gasification of coal with production of high-quality syngas in a simulated pilot system for in situ gasification.Appl. Energy 2014, 131, 9–19. https://doi.org/10.1016/j.apenergy.2014.06.001

[11] Daggupati, S.; Mandapati, R.N.; Mahajani, S.M.; Ganesh, A.; Mathur, D.K.; Sharma, R.K.; Aghalayam, P. Laboratory studies on combustion cavity growth in lignite coal blocks in the context of underground coal gasification. Energy 2010, 35, 2374–2386. https://doi.org/10.1016/j.energy.2010.02.015

[12] Perkins, G. and V. Sahajwalla, Steady-State Model for Estimating Gas Production from Underground Coal Gasification. Energy & Fuels, 2008. 22(6): p. 3902-3914. https://doi.org/10.1021/ef8001444

[13] Perkins, G. and V. Sahajwalla, A Numerical Study of the Effects of Operating Conditions and Coal Properties on Cavity Growth in Underground Coal Gasification. Energy & Fuels, 2006. 20(2): p. 81 - 88. https://doi.org/10.1021/ef050242q

[14] Yang, L., Study on the model experiment and numerical simulation for underground coal gasification. Fuel, 2004. 83(4/5): p. 573-584.https://doi.org/10.1016/j.fuel.2003.08.011

[15] Khadse, A.N., et al., Reactor Model for the Underground Coal Gasification (UCG) Channel. International Journal of Chemical Reactor Engineering, 2006. 4(1). https://doi.org/10.2202/1542-6580.1351

[16] Nourozieh, H., et al., Simulation Study of Underground Coal Gasification in Alberta Reservoirs: Geological Structure and Process Modeling. Energy & Fuels, 2010. 24(MAY-JUN.): p. 3540-3550. https://doi.org/10.1016/j.cherd.2012.11.008

[17] Daggupati, S., et al., Compartment Modeling for Flow Characterization of Underground Coal Gasification Cavity. Industrial & Engineering Chemistry Research, 2011. 50(1): p. 277-290. https://doi.org/10.1021/ie101307k

[18] Sarndani, G., et al., A process model for underground coal gasification – Part-III: Parametric studies and UCG process performance. Fuel, 2018. 234(DEC.15): p. 392-405. https://doi.org/10.1016/j.fuel.2018.07.011

[19] Samdani, G., et al., A process model for underground coal gasification – Part-II growth of outflow channel. Fuel, 2016. 181: p. 587-599.https://doi.org/10.1016/j.fuel.2016.05.017

[20] Samdani, G., et al., A process model for underground coal gasification – Part-I: Cavity growth. Fuel, 2016. 181(oct.1): p. 690-703.https://doi.org/10.1016/j.fuel.2016.05.020

[21] Gao, W., et al., Simulation of underground coal gasification based on a coupled thermal-hydraulic-chemical model. Combustion theory and modelling, 2022(1): p. 26. https://doi.org/10.1080/13647830.2021.1992507

[22] Xin, L., et al., Theoretical research on heat transfer law during underground coal gasification channel extension process. International Journal of Heat and Mass Transfer, 2019. 142(OCT.): p. 118409.1-118409.14.https://doi.org/10.1016/j.ijheatmasstransfer.2019.07.059

[23] Shahbazi, M., M. Najafi and M.F. Marji, On the mitigating environmental aspects of a vertical well in underground coal gasification method. Mitigation and Adaptation Strategies for Global Change, 2019. 24. https://doi.org/10.1007/s11027-018-9816-x

[24] Cheng W , Xin L , Wang G ,et al.Analytical research on dynamic temperature field of overburden in goaf fire-area under piecewise-linear third boundary condition[J].International Journal of Heat & Mass Transfer, 2015, 90(nov.):812-824.DOI:10.1016/j.ijheatmasstransfer.2015.07.012.

[25] Najafi, M., et al., Prediction of cavity growth rate during underground coal gasification using multiple regression analysis. International Journal of Coal Science & Technology, 2015. 2(004): p. 318-324.https://doi.org/10.1007/s40789-015-0095-9

[26] Blinderman, M.S., D.N. Saulov and A.Y. Klimenko, Forward and reverse combustion linking in underground coal gasification. Energy, 2008. 33(3): p. 446-454. https://doi.org/10.1016/j.energy.2007.10.004

[27] Hsu, C., et al., Investigation of cavity formation in lump coal in the context of underground coal gasification. Journal of the Southern African Institute of Mining & Metallurgy, 2014. 114(4): p. 305-309. DOI:10.1016/j.energy.2010.02.015.

[28] Liu, X., G. Guo and H. Li, Study on the Propagation Law of Temperature Field in Surrounding

Rock of Underground Coal Gasification(UCG) Combustion Cavity Based on Dynamic Thermal Parameters. Results in Physics, 2019. 12. https://doi.org/10.1016/j.rinp.2019.02.006

[29] Prabu, V. and S. Jayanti, Heat-affected zone analysis of high ash coals during ex situ experimental simulation of underground coal gasification. Fuel, 2014. 123(may 1): p. 167-174. https://doi.org/10.1016/j.fuel.2014.01.035

[30] Prabu, V. and S. Jayanti, Simulation of cavity formation in underground coal gasification using bore hole combustion experiments. Energy, 2011. 36(10): p. 5854-5864. https://doi.org/10.1016/j.energy.2011.08.037

[31] Su, F.Q., et al., Monitoring and evaluation of simulated underground coal gasification in an ex-situ experimental artificial coal seam system. Applied Energy, 2018. 223(AUG.1): p. 82-92. https://doi.org/10.1016/j.apenergy.2018.04.045

[32] Su F Q , Zhang T , Wu J B ,et al.Energy recovery evaluation and temperature field research of underground coal gasification under different oxygen concentrations[J].Fuel: A journal of fuel science, 2022. https://doi.org/10.1016/j.fuel.2022.125389

[33] Fa-qiang, et al., Evaluation of Coal Combustion Zone and Gas Energy Recovery for Underground Coal Gasification (UCG) Process. Energy & Fuels, 2016. 31(1): p. 154-169. https://doi.org/10.1021/acs.energyfuels.6b01922

[34] Su, F.Q., et al., Monitoring of coal fracturing in underground coal gasification by acoustic emission techniques. Applied Energy, 2017. 189(MAR.1): p. 142-156. https://doi.org/10.1016/j.apenergy.2016.11.082

[35] Tribikram Kundu. Acoustic source localization (Ultrasonics, vol. 54, issue 1) (2013). https://doi.org/10.1016/j.ultras.2013.06.009